Chinese Journal of
POLYMER SCIENCE

REVIEW

https://doi.org/10.1007/s10118-026-3884-2
Chinese J. Polym. Sci.

Flexible Freestanding Chiroptical Films: Construction Strategies, Chiroptical Programming, and Applications

Pan-Yi Xi[a,b,†], Sheng-Dan Xie[a,†], Yi-Yang Kang[a], and Xi-Chong Ye[a,c,d*]

[a] *Shaanxi International Research Center for Soft Matter, State Key Laboratory for Mechanical Behavior of Materials, Xi'an Jiaotong University, Xi'an 710049, China*
[b] *National Demonstration Center for Experimental Light Chemistry Engineering Education, College of Bioresources Chemical and Materials Engineering, Shaanxi University of Science and Technology, Xi'an 710021, China*
[c] *Institute of New Concept Sensors and Molecular Materials, Shaanxi Provincial Key Laboratory of New Concept Sensors and Molecular Materials, Xi'an Jiaotong University, Xi'an 710049, China*
[d] *Xi'an Key Laboratory of Sustainable Polymer Materials, Xi'an Jiaotong University, Xi'an 710049, China*

Abstract Flexible freestanding chiroptical films (FFCFs) are substrate-independent, mechanically deformable films that retain structural integrity and measurable chiroptical activity. Their substrate independence and mechanical adaptability enable conformal integration into lightweight chiral optical devices. However, relevant studies remain dispersed across multiple research fields, and FFCFs have not yet been consolidated within a unified material framework. Herein, we define the scope of FFCFs and clarify the key chiroptical parameters, measurement protocols, and reliability considerations required for their evaluation. This review focuses on four representative construction strategies: multicomponent coupling, helical assembly, twisted stacking, and geometric microstructuring. For each strategy, we examine how chirality is generated, transferred, and amplified, together with how mechanical deformability, structural states, and chiroptical responses can be regulated. We then discuss applications in encryption and anti-counterfeiting, display and visualization, detection, recognition, and sensing. Particular attention is given to anisotropy-induced signal artifacts and limited large-area reproducibility, which continue to impede reliable characterization and practical fabrication. By consolidating these advances, this review aims to establish FFCFs as a distinct material platform and provide a coherent framework for their design, characterization, and application.

Keywords Chiroptical films; Freestanding films; Flexible optics; Optical activity; Optical devices

Citation: Xi, P. Y.; Xie, S. D.; Kang, Y. Y.; Ye, X. C. Flexible freestanding chiroptical films: construction strategies, chiroptical programming, and applications. *Chinese J. Polym. Sci.* https://doi.org/10.1007/s10118-026-3884-2

INTRODUCTION

Chirality denotes the property of an object that cannot be superimposed on its mirror image, and gives rise to dissymmetric interactions with left- and right-handed circularly polarized light (LCP and RCP).[1,2] Chiroptical responses may arise from intrinsic molecular asymmetry or from higher-order structural chirality.[3] In condensed-state materials, supramolecular assembly,[4,5] liquid-crystalline ordering,[6–8] interlayer twisting,[9,10] and mesoscale geometric organization[11,12] enable chirality to be transferred, amplified, and programmed across multiple length scales. Practical chiroptical functions require these ordered chiral structures to be stabilized within continuous and well-defined material architectures.[13–15]

Among such architectures, thin films are particularly well-suited for generating controllable chiroptical outputs.[16] Compared to bulk materials and powders, thin films provide a continuous quasi-two-dimensional geometry in which the thickness, constituent alignment, hierarchical order, and interfacial structure can be systematically controlled.[17] Their planar form also establishes a well-defined optical propagation geometry, facilitating the interpretation and tuning of the thickness- and orientation-dependent responses.[18] As a result, thin films can support diverse chiroptical functions, including circular dichroism (CD),[19,20] circularly polarized luminescence (CPL),[21,22] and circular polarization-selective reflection.[23,24] However, many chiral thin films have been fabricated and used on permanent substrates, which limits their independent handling, deformation, transfer, and multilayer reconfiguration.

Flexible freestanding chiroptical films (FFCFs) address this constraint by retaining a continuous morphology, mechanical integrity, and measurable chiroptical responses without a permanent supporting substrate. Removing the permanent substrate can eliminate substrate-derived absorption and birefringence, and avoid substrate-related scattering and reflection, thereby facilitating the assignment of film-intrinsic chiroptical responses. More importantly, depending on their composition and mechanical properties, FFCFs can be inde-

* Corresponding author, E-mail: xcye917@xjtu.edu.cn
† These authors contributed equally to this work.
Special Topic: Chirality in Polymers
Received August 4, 2026; Accepted September 9, 2026; Published online November 17, 2026

© Chinese Chemical Society
Institute of Chemistry, Chinese Academy of Sciences

pendently transferred, cut, bent, stretched, folded or stacked.[16,25,26] These capabilities support the mechanical modulation of chiroptical responses and construction of reconfigurable multilayer architectures. Their low areal mass and small thickness further favor lightweight and miniaturized devices, whereas their flexibility enables conformal integration.[16]

Despite the rapid development of chiral thin-film materials, FFCFs have not yet been systematically reviewed as distinct material platforms. Relevant FFCF studies have been dispersed among reviews devoted to chiral photonic films,[14,27,28] chiral liquid-crystalline materials,[29] CPL materials,[18,30–32] and chiral metasurfaces.[16,33,34] This fragmentation has left their scope, performance metrics, construction principles, and form-dependent functional advantages insufficiently consolidated. Therefore, this review defines the scope of FFCFs and summarizes the key chiroptical parameters, characterization methods, and reliability considerations for film state evaluation. The reported systems are then organized according to the four representative strategies used to construct and program freestanding chiral structures. Their applications were further discussed in terms of encryption, display, and detection, *etc*. Finally, we examined two cross-cutting challenges: reliable assignment of chiroptical signals and reproducible fabrication over large areas, and outlined priorities for scalable processing, durability evaluation, and functional integration (Fig. 1).[8,12,20,35–43]

FUNDAMENTALS OF FFCFS

Scope

In this review, FFCFs are defined as substrate-independent, mechanically deformable films that retain a continuous morphology, structural integrity, and measurable chiroptical activity. The key distinguishing feature of conventional chiral coatings is that they can maintain a continuous film morphology and measurable chiroptical response after removal from the fabrication substrate, which relies on a permanent carrier for structural support. Therefore, the freestanding nature of FFCFs offers distinct advantages in terms of processing, optical characterization, mechanical reconfiguration, and device integration. It enables substrate-free post-treatment, cutting, and transfer; avoids substrate-induced optical artifacts in intrinsic chiroptical measurements; permits diverse macroscopic deformations without rigid-substrate confinement; and facilitates conformal attachment, stacking, and flexible integration with heterogeneous functional systems. The use of temporary substrates during fabrication or sample holders for measurement did not affect this classification. Flexibility should be demonstrated by nondestructive macroscopic deformations, such as bending, folding, twisting, or stretching.[44–46] Solutions, powders, isolated crystals, and discontinuous micro- or nanostructures are excluded because they lack a continuous film morphology, while rigid self-supporting sheets are excluded because they lack flexibility. Flexible films containing chiral components, but exhibiting no measurable

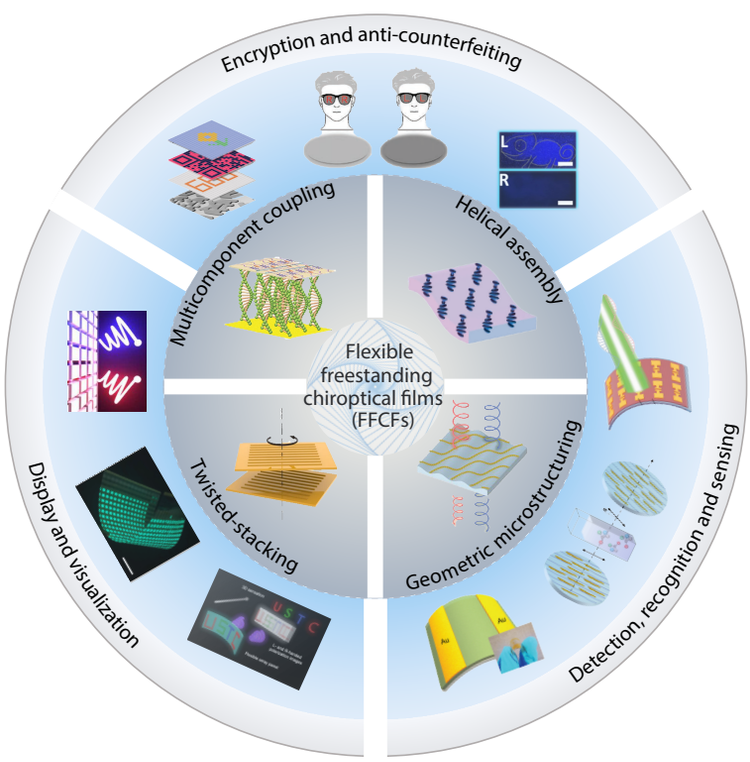


Fig. 1 Schematic overview of the four representative construction strategies and major application categories of flexible freestanding chiroptical films (FFCFs) (Reproduced with permission from Ref. [8]; Copyright (2023), Wiley; Ref. [12]; Copyright (2025), Wiley; Ref. [20]; Copyright (2020), Wiley; Ref. [35]; Copyright (2025), Wiley; Ref. [36]; Copyright (2024), Wiley; Ref. [37]; Copyright (2023), Wiley; Ref. [38]; Copyright (2023), Wiley; Ref. [39]; Copyright (2023), Springer Nature; Ref. [40]; Copyright (2023), Springer Nature; Ref. [41]; Copyright (2025), Springer Nature; Ref. [42]; Copyright (2025), The American Association for the Advancement of Science; Ref. [43]; Copyright (2023), The American Association for the Advancement of Science.)

https://doi.org/10.1007/s10118-026-3884-2

Table 1 Scope assessment of representative chiral material forms.

Material form	Classification	Scope criterion
Multicomponent blended films	Conditionally included	Intercomponent interactions formed upon blending alter, amplify, or transfer chirality
Chiral photonic films	Conditionally included	Independent handling and macroscopic flexibility are demonstrated after substrate removal
Chiral liquid-crystal networks	Conditionally included	The film can be removed from the fabrication substrate while retaining its structure and chiroptical response
Twisted stacks of flexible films	Conditionally included	The assembled stack is freestanding and the stable interlayer twist generates the chiroptical response
Ultrathin films and metasurfaces	Conditionally included	Transferability alone is insufficient; freestanding integrity and flexibility must also be demonstrated
Chiral hydrogel and elastomer films	Conditionally included	An integrated membrane is maintained under its operating conditions, discontinuous gel assemblies are excluded
Chiral coatings on substrates	Excluded	The chiroptical layer depends on a permanent external carrier
Rigid chiral sheets or plates	Excluded	They do not meet the flexibility criterion

film-state chiroptical responses, are beyond the scope of this review. For multicomponent blended films, simple physical blending is insufficient; inter-component interactions are required to modify, amplify, or transfer chirality. Representative included, excluded, and boundary cases are summarized in Table 1. All the conditionally included systems must satisfy the general definition of FFCFs provided above.

Chiroptical Parameters

FFCFs can exhibit handedness-dependent responses in extinction, emission, reflection, and transmission, as well as electrical, thermal, and mechanical outputs generated through optical transduction.[24,35,47] Formally, circular dichroism (CD) describes the differential absorption of left- and right-handed circularly polarized light.[16] For thin films, however, the attenuation inferred from transmitted intensity measurements can also include scattering and interfacial reflection contributions. Therefore, the measured CD signal may represent differential extinction rather than pure differential absorption.[16] Throughout this review, $A = -\lg T$ denotes the apparent absorbance, or extinction, derived from transmission measurements. The corresponding differential extinction is defined as $\Delta A = A_L - A_R$, where A_L and A_R are obtained upon LCP and RCP illumination, respectively. Commercial CD instruments commonly convert ΔA into ellipticity θ: $\theta\,(\mathrm{mdeg}) = 32982 \times \Delta A$.[48] Despite the possible contribution of non-absorptive losses, the normalized asymmetry is conventionally reported as the absorption dissymmetry factor g_{abs}:

$$g_{abs} = \frac{2(A_L - A_R)}{A_L + A_R} = \frac{\Delta A}{\overline{A}} = \frac{\theta(\mathrm{mdeg})}{32982\overline{A}} \quad (1)$$

where $\overline{A}$ is the average value of A_L and A_R. Under this convention, a positive g_{abs} indicates a greater apparent extinction under LCP illumination, whereas a negative value indicates a greater extinction under RCP illumination. Its absolute value quantifies the normalized chiroptical asymmetry. The theoretical range of g_{abs} is from −2 to +2.

For emissive FFCFs, the circularly polarized luminescence is similarly quantified by the luminescence dissymmetry factor:

$$g_{lum} = 2\frac{I_L - I_R}{I_L + I_R} \quad (2)$$

where I_L and I_R are the LCP and RCP emission intensities, respectively. Positive and negative values indicated preferential LCP and RCP emissions, respectively. The theoretical range also ranges from −2 to +2. Because g_{lum} describes polarization asymmetry rather than total emission efficiency, it should be considered together with emission intensity or photoluminescence quantum yield (PLQY). Therefore, some studies have used a CPL figure of merit (FOM), defined as FOM = $|g_{lum}|$·PLQY to jointly evaluate emission dissymmetry and photoluminescence efficiency.[49]

For chiral photonic films, particularly chiral nematic (cholesteric) structures, the periodic helical architecture produces Bragg reflection, and thereby selectively reflects one circular polarization while preferentially transmitting the opposite handedness.[27,50] For an ideal uniformly aligned helical structure, the central reflection wavelength (λ_0) is determined by:

$$\lambda_0 = \overline{n}P\cos\theta \quad (3)$$

where P is the helical pitch, $\overline{n}$ is the average refractive index, and θ is the internal propagation angle between the propagation direction and the helical axis. Conventional CD ellipticity and g_{abs} are useful for characterizing the chiroptical response of such materials; however, they do not directly quantify the difference in optical power transmitted through the film and delivered to a downstream functional component. This distinction becomes relevant in transmission-based devices, such as photothermal, photodetection, or photoactuation systems, whose responses are governed directly by the transmitted optical power. For this purpose, we introduce an operational optical power asymmetry factor, g_{op}, to quantify the difference in transmitted power under LCP and RCP illumination. g_{op} is not a generally established chiroptical dissymmetry factor and is not intended to replace g_{abs}. It serves as a device-level metric for evaluating handedness-dependent optical power delivery under the actual operating conditions of a transmission-based photonic system. The normalized transmittances are defined as $\phi_{R/L} = I_{R/L}/I_0$, where I_0 is the incident optical power or power density and $I_{R/L}$ is the transmitted power under LCP and RCP illumination. Accordingly,

$$g_{op} = \frac{2(\phi_L - \phi_R)}{\phi_L + \phi_R} \quad (4)$$

The value of g_{op} ranged from −2 to +2. Because g_{op} is calculated from linear transmittance ratios, whereas g_{abs} is derived from logarithmic apparent absorbance or extinction, the two parameters describe different aspects of chiroptical performance and their numerical values should not be compared

https://doi.org/10.1007/s10118-026-3884-2

directly.

For FFCFs that convert circular polarization-induced asymmetry into electrical, thermal, or mechanical signals, both the absolute outputs upon LCP and RCP excitation, as well as their difference or well-defined normalized asymmetry, should be reported. These chiral-contrast metrics should be complemented by response-specific performance metrics, such as responsivity and detectivity for photoelectric conversion, handedness-dependent thermal contrast for photothermal conversion, and deformation amplitude, curvature, response time, and recovery time for optical actuation.

Characterization Methods

Chiroptical characterization should be selected according to the response mode and measurement objective. CD and CPL spectroscopies were used for apparent differential extinction and circularly polarized emission, respectively. For anisotropic films, polarization-dependent absorption and fluorescence should be independently measured using absorption and fluorescence spectrometers equipped with linear polarizers to quantify linear dichroism (LD) and linearly polarized emission. The linear birefringence and optical retardance can be quantified using spectroscopic ellipsometry. Stokes polarimetry is used when the complete polarization state of the output light must be resolved, whereas Mueller-matrix polarimetry/ellipsometry is required to characterize the polarization-transforming and depolarizing properties of the film itself.

As FFCFs can exhibit pronounced anisotropy and nonplanar deformation, their measurements are susceptible to artifacts arising from thickness nonuniformity, surface roughness, scattering, warpage, wrinkles, and linear anisotropy.[51,52] Notably, the dominant artifacts vary with film construction strategies: LD and linear birefringence (LB) represent major sources of measurement artifacts for twisted-stacking systems, whereas scattering, domain misalignment, and thickness nonuniformity are more critical for helical photonic films. Therefore, the reliability of the measured chiroptical response should be examined through sample rotation about the optical axis, front-back reversal, and measurements at multiple positions or on independent specimens.[52] Spatially resolved mapping is preferable when the large-area uniformity is evaluated. Integrating-sphere measurements can help evaluate scattering contributions and retrieve the total transmission or reflection, whereas baseline correction removes only instrumental or reference backgrounds. Baseline subtraction cannot eliminate sample-derived scattering, linear anisotropy, or depolarization. For strongly anisotropic films, Mueller matrix decomposition is preferred to distinguish circular dichroism and birefringence from linear dichroism and birefringence.[39,53]

Structural and mechanical characterizations should establish how the film architecture governs its chiroptical response. Microscopy, diffraction, and scattering techniques can be selectively employed to resolve the molecular alignment, helical pitch, layered order, interfacial twist, and mesoscale geometry. Mechanical testing should reflect the intended deformation mode, and deformation conditions should be quantified using appropriate parameters, such as strain, bending radius or curvature, loading rate, and cycle number. The corresponding chiroptical response should be monitored before, during, or after deformation to determine its retention, reversibility, and fatigue stability. For large-area films, spatial uniformity before and after deformation should also be assessed.[13]

CONSTRUCTION AND CHIROPTICAL PROGRAMMING

The construction of FFCFs generally relies on the conversion of molecular chirality, optical anisotropy, or geometric asymmetry into stable macroscopic chiroptical responses. Herein, we classify the reported design principles into four representative strategies: multicomponent coupling, helical assembly, twisted stacking, and geometric microstructuring. For each strategy, we summarize the recent progress, clarify the mechanisms of chirality generation and amplification, and discuss their advantages and limitations regarding optical tunability, structural programmability, mechanical deformability, and scalable fabrication.

Multicomponent Coupling Strategies

Multicomponent coupling strategies are used to construct FFCFs by integrating two or more functional components through specific noncovalent interactions (Fig. 2a). Unlike simple physical blending, such interactions regulate the molecular conformation, aggregation, and intercomponent organization, thereby enabling chirality transfer, amplification, and dynamic chiroptical modulation.[36,54]

Hydrogen bonding is particularly useful for immobilizing functional components in polymer networks while retaining their reversible responses to external stimuli. Duan *et al.* incorporated trace amounts of axially chiral 1,1'-bi-2-naphthol (BINOL) units into a polyurethane elastomer, where hydrogen bonding, π-π interactions, and microphase organization cooperatively produced long-range ordered domains. The resulting film exhibited a $|g_{lum}|$ of 2.30×10^{-2} and a fracture toughness of (56.28±3.9) MJ·m^{-3} (Fig. 2b).[36] Guo *et al.* embedded chiral phosphorescent carbazole derivatives in poly(vinyl alcohol) (PVA), where a dynamic hydrogen-bonding network stabilized the triplet excited states and could be reversibly reorganized by exposure to water vapor and heating. The flexible films showed a color-tunable circularly polarized afterglow with a lifetime of up to 3.35 s, quantum yield of 25.0%, and $|g_{lum}|$ of up to 0.05.[55] In a ternary cellulose nanocrystal (CNC)/1,5-dihydroxynaphthalene/polyurethane system, a hydrogen-bond-rich polyurethane network and π–H interactions direct the formation of feather-like nanostructures, producing flexible films with amplified and multimodally responsive CPL.[56] Hydrogen bonding can also stabilize long-lived excited states by restricting molecular motion and suppressing nonradiative decay. This effect enabled simultaneous circularly polarized thermally activated delayed fluorescence and room-temperature phosphorescence in the acridine-flavin/CNC/PVA films.[57] Dynamic hydrogen bonds in egg-albumen/gelatin supramolecular glasses further combine molecular confinement with network toughening to produce flexible films with tunable circularly polarized afterglow.[58]

Coordination interactions can reorganize chiral assemblies and regulate their chiroptical response. Li *et al.* reported chiral flexible peptide films formed through coordination inter-

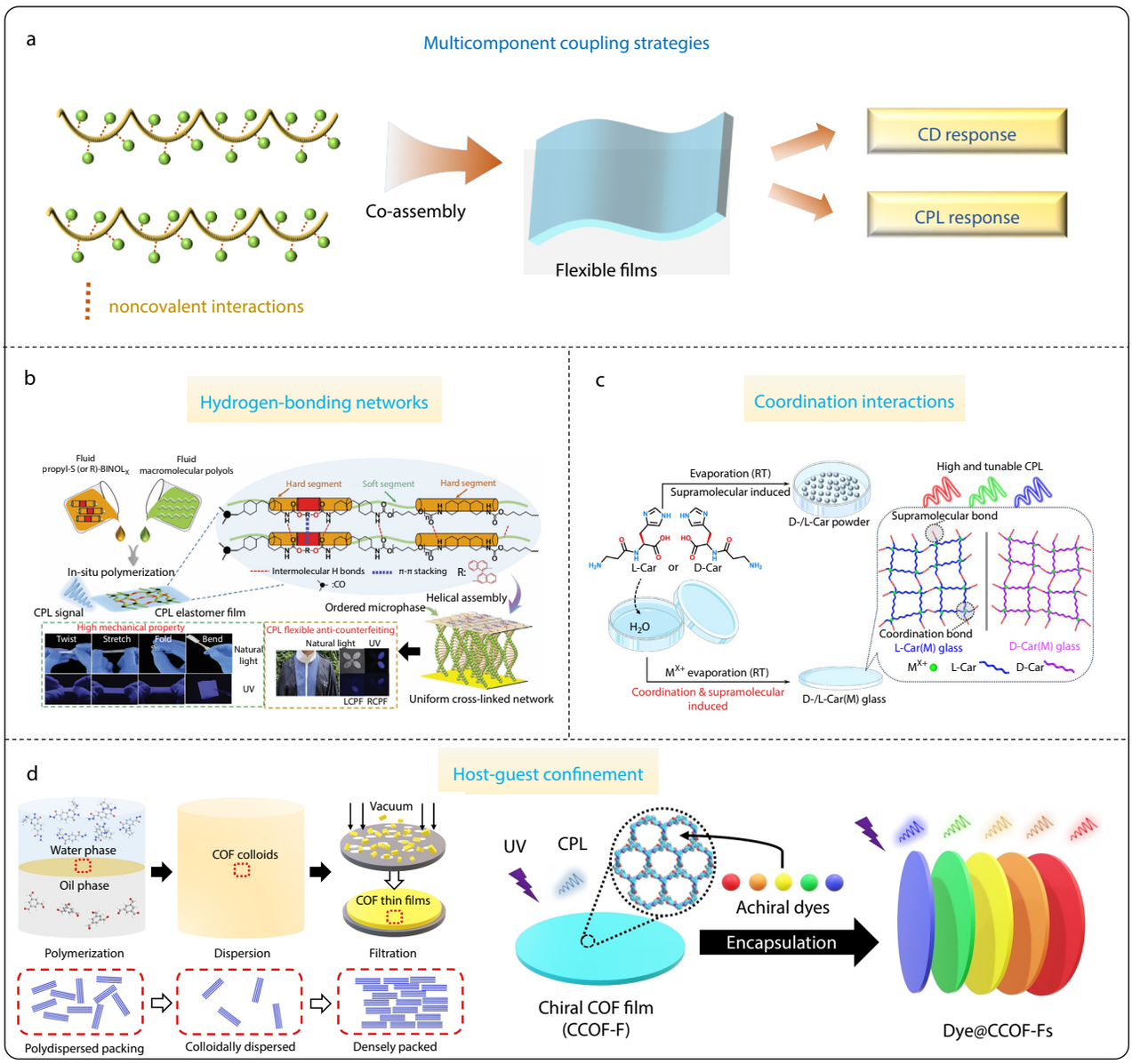


Fig. 2 (a) Schematic illustration of multicomponent coupling strategies, in which two or more functional components co-assemble through noncovalent interactions to form FFCFs with CD or CPL responses; (b) Hydrogen-bonded supramolecular polyurethane networks undergo microphase ordering and helical assembly to form flexible CPL elastomers (Reproduced with permission from Ref. [36]; Copyright (2024), Wiley); (c) D-/L-carnosine molecules self-assemble through supramolecular interactions and further coordinate with metal ions to form chiral glasses (Reproduced with permission from Ref. [59]; Copyright (2026), Wiley); (d) Confinement of achiral dyes within oriented chiral COF pores transfers chirality to the guest molecules and gives rise to full-color CPL (Reproduced with permission from Ref. [54]; Copyright (2024), Wiley).

actions between carnosine enantiomers and metal ions (Zn^{2+}, Eu^{3+}, Tb^{3+}, and Gd^{3+}). The resulting glasses exhibited > 90% transparency, easy processability, ambient self-healing, multicolor emission, and a high CPL response with g_{lum} up to 0.29 (Fig. 2c).[59] This type of interaction is also widely used to construct chiral supramolecular gels and assemblies, many of which exhibit robust structures and pronounced or tunable chiroptical responses.[60,61] These interactions can promote chirality transfer, hierarchical assembly, and, in some cases, energy transfer between different components. However, their ability to form mechanically robust, freestanding, and flexible films has not been demonstrated. Therefore, they were not included here as FFCFs, although they provide useful molecular and supramolecular design principles for future freestanding chiroptical films.

Host-guest interactions can instead transfer chirality through an ordered porous environment. Tang *et al.* fabricated freestanding chiral COF films using a polymerization-dispersion-filtration process. The films contained preferentially oriented chiral pores and exhibited intrinsic diffuse-reflectance CD and CPL. Adsorption of different achiral fluorescent dyes within these pores enabled simultaneous chirality and energy transfer from the framework to the guests, producing a full-color solid-state CPL with $|g_{lum}|$ up to 0.072 (Fig.

2d).[54] Related studies confined chiral titanium-oxo clusters or chiral carbon nanodots within fluorescent MOF thin films to generate or enhance CPL.[62,63] Molecularly imprinted polymer films provide reusable chiral cavities for loading different emitters and generating full-color CPL.[64]

Overall, multicomponent coupling offers a modular route to FFCFs because the chirality, emission, and mechanical properties can be adjusted through component selection and coupling modes. The reversibility of non-covalent interactions also enables responsive chiroptical modulation. Compared with other strategies, multicomponent coupling offers broad chemical and compositional design freedom; however, achieving a uniform macroscopic chiroptical response requires precise organization of the constituent components. In a freestanding format, the film-forming matrix can simultaneously provide mechanical support and participate in chiroptical functions, enabling dynamic modulation and mechanical deformation without the constraint or optical interference of a permanent substrate. However, the dynamic nature of these interactions makes the resulting structures sensitive to the composition, processing history, and environmental conditions. Inadequate component organization,[56] insufficient control over host-guest interactions,[54] phase separation,[36] aggregation-induced quenching,[57] and light scattering[54] may further compromise optical uniformity and long-term stability. Improving spatial control, mechanistic understanding, and large-area reproducibility, while retaining dynamic tunability, remains a central challenge.

Helical Assembly Strategies

Helical assembly strategies construct FFCFs by organizing molecular or nanoscale building blocks into continuous long-range helical phases[7] or frameworks.[65] Such hierarchical ordering amplifies local chirality into macroscopic chiroptical responses, whereas variations in helical pitch, handedness, and structural order provide direct routes for tuning circularly polarized reflection, absorption, and emission (Fig. 3a).[65]

Cholesteric liquid-crystal elastomers (CLCEs) couple their helical photonic structures with the deformability of crosslinked polymer networks. Mechanical deformation changes the helical pitch and therefore shifts the reflection band. Kizhakidathazhath *et al.* developed an anisotropic deswelling method to prepare large-area CLCE films with a uniform planar alignment. Uniaxial or biaxial stretching compresses the helix along the film thickness and produces an immediate, reversible shift of the reflection band across the visible range, from red to blue.[7] Dynamic covalent networks allow the helical structures to be reconFig.d or fixed after deformation. Ma *et al.* incorporated boronic ester bonds into a main-chain CLCE network. The films retained reversible mechanochromism across the full visible range, while bond exchange enabled shape reprogramming, interfacial self-healing, and the reconstruction of damaged optical regions (Fig. 3b).[24] Liu *et al.* introduced light-responsive diselenide bonds in CLCE films. Under mechanical deformation and light irradiation, the diselenide exchange reorganized the network and allowed deformation-induced changes in the helical pitch and film thickness to be retained after unloading. This mechanism enables the color patterns to be written, erased, and rewritten.[66] Hussain *et al.* reprogrammed the helical pitch and handedness within a single CLCE film, enabling control over both the reflection wavelength and circular-polarization selectivity.[67] Kim *et al.* used pneumatic inflation to impose biaxial strain on patterned CLCE membranes, shifting the reflection band from near-infrared to ultraviolet at strains below 20%.[6] Nam *et al.* coupled CLCE films with electrically driven elastomer actuators. Electrically generated expansion or contraction produces reversible blue or red shifts of the reflection band, respectively.[68]

Helical templating transcribes chiral architectures into stable porous frameworks while preserving their handedness and spatial periodicity. Shi *et al.* photopolymerized reactive mesogens within a chiral nematic phase and removed nonreactive liquid crystal components. The resulting soft photonic crystal film retained continuous helical nanopores and a tunable circular polarization-selective reflection band. Different fluorescent dyes were repeatedly loaded into and eluted from the pores, producing multicolor and white CPL with $|g_{lum}|$ up to 0.47, while suppressing dye aggregation (Fig. 3c).[40] This templating concept has also been extended to inorganic emitters. Choi *et al.* grew nonchiral two-dimensional hybrid perovskites inside nanoporous cholesteric polymer templates. The induced CD and CPL persisted even when the perovskite emission lay outside the reflection band, indicating chirality transfer from the pore structure rather than a simple selective reflection.[69] Qin *et al.* further confined full-color-emitting carbon quantum dots within helical nanopores. Confinement simultaneously induced CPL and suppressed aggregation-caused quenching, yielding $|g_{lum}|$ up to 0.48 and PLQY up to 92% (Fig. 3d).[65]

Overall, the helical assembly translates molecular or nanoscale chirality into long-range periodic order across the film. This structural amplification can generate circularly polarized reflection, strong CD, or CPL, whereas the pitch, handedness, and hierarchical order can be tuned by strain, light, temperature, or solvent. Unlike multicomponent coupling, helical assembly provides a more direct relationship between structural parameters and chiroptical responses, allowing the optical properties to be tuned through controlled variation of the helical architecture. In freestanding elastomeric or porous films, such architectures can undergo deformation or transfer while preserving their helical order, enabling the mechanical modulation of the chiroptical response. The absence of a rigid supporting substrate further facilitates its integration with actuators and other flexible components. However, the same long-range order also renders these films sensitive to structural defects. Pitch gradients, domain boundaries, thickness variations, and imperfect alignment can broaden the reflection bands and weaken polarization selectivity. Maintaining uniform helical order, mechanical integrity, and dynamic tunability over large areas remains a central challenge.

Twisted-stacking Strategies

Twisted-stacking strategies are used to construct FFCFs by stacking anisotropic layers with controlled angular offsets. Each layer may exhibit linear dichroism, linear birefringence, linearly polarized emission, or anisotropic optical resonance. When the principal optical axes of the adjacent layers are twisted relative to each other, the stacked structure can interact differently with left- and right-handed circularly polarized light (Fig. 4a). This ge-

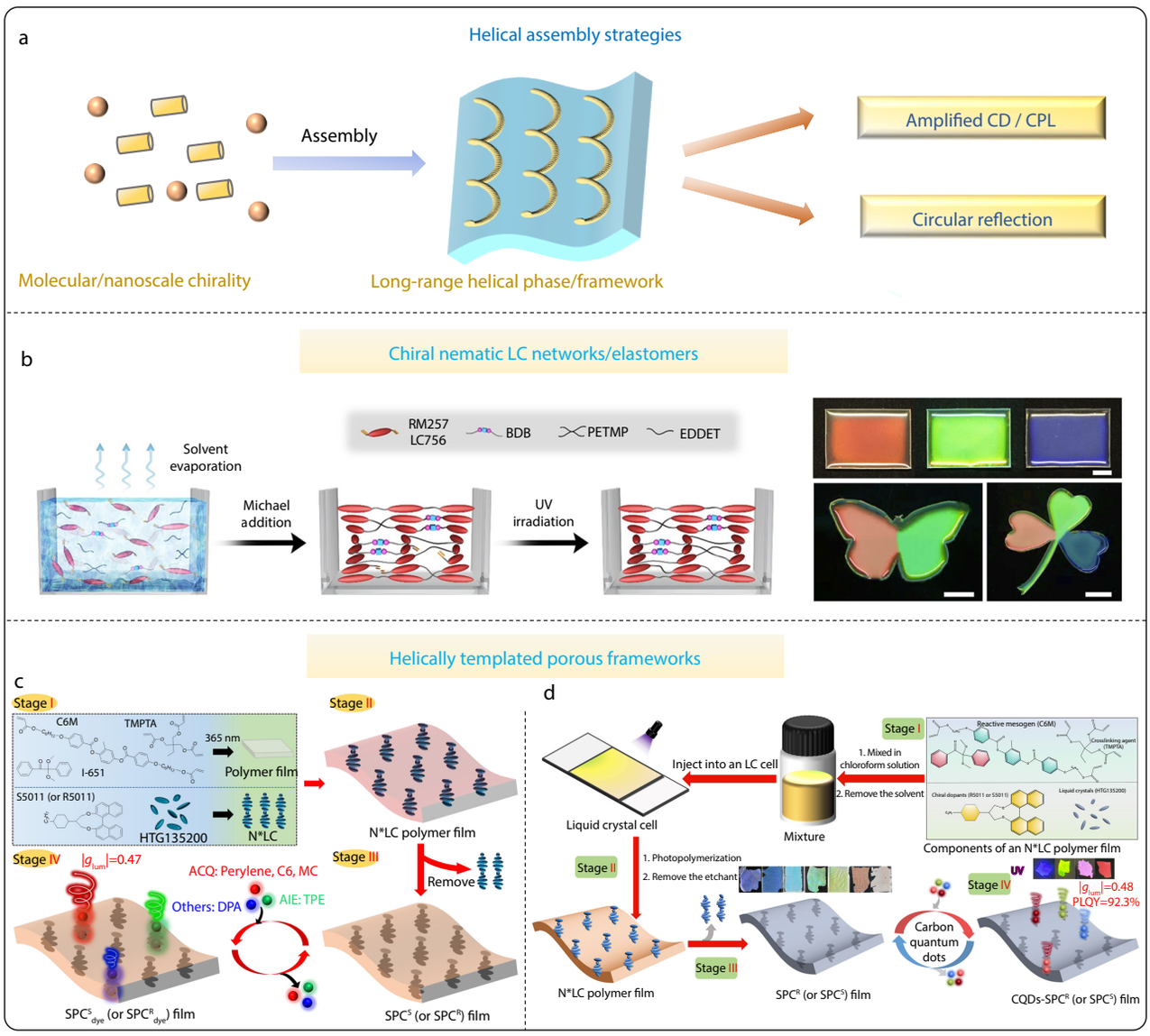


Fig. 3 (a) Molecular or nanoscale chirality is transferred into long-range helical phases or frameworks, yielding amplified chiroptical responses; (b) Cholesteric liquid-crystal elastomers fabricated through sequential thiol-acrylate Michael addition and photopolymerization, yielding multicolor structural reflection and programmable photonic films (Reproduced with permission from Ref. [24]; Copyright (2022), Wiley); (c) Chiral photonic polymer templates are fabricated from cholesteric liquid crystals and converted into recyclable soft photonic crystal films, in which the incorporation of luminescent molecules enables CPL (Reproduced with permission from Ref. [40]; Copyright (2023), Springer Nature); (d) Helically templated porous polymer frameworks that confine luminescent carbon quantum dots to produce full-color CPL (Reproduced with permission from Ref. [65]; Copyright (2026), Wiley).

ometry-driven approach enables macroscopic chiroptical responses from achiral or weakly chiral building blocks, without relying on continuous helical phases.[39,70]

Twisted-stacking strategies can generate CD signals by coupling linear dichroism (LD) with phase retardation. Xie *et al.* stacked a transparent anisotropic PVA layer with an oriented-dye-containing PVA layer. The transparent layer provided linear birefringence, whereas the dye layer provided linear dichroism. When their optical axes were twisted, the LCP and RCP were converted into different linear polarization states and therefore experienced different absorptions in the dye layer. Using robotic fabrication and machine-learning-based inverse design, the authors optimized the film thickness, strain, dye absorption, and twist angle, producing flexible chiral films with gabs values up to 1.9 across the visible range (Fig. 4b).[39] This concept has also been extended to plasmonic metasurfaces assembled from achiral nanoparticles. Probst *et al.* fabricated dense Au nanoparticle chains on elastomeric substrates and stacked two-chain arrays at controlled crossing angles. The interlayer plasmonic coupling generated a strong CD of up to 11°, whereas the open interlayer gaps provided accessible regions of superchiral electromagnetic fields for chiral analytes (Fig. 4c). Restacking and local mechanical compression allowed the sign, magnitude, and spectral position of the CD response to be tuned.[45] Related systems have expanded the spectral range and mechanical tunability of

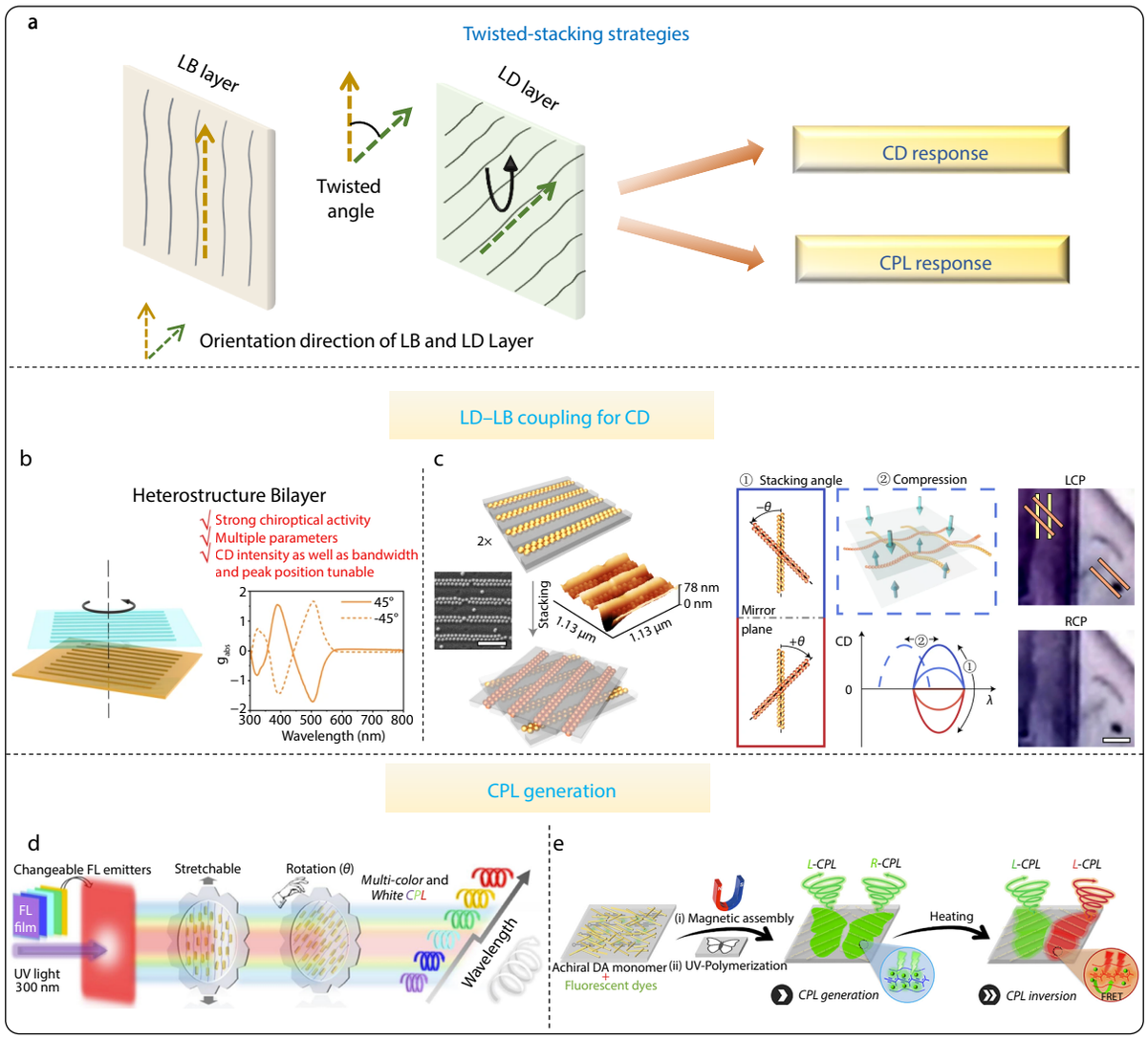


Fig. 4 (a) Twisted-stacking layers generate CD and CPL through interlayer optical coupling; (b) Twisted heterobilayers with tunable CD magnitude, bandwidth, and spectral position (Reproduced with permission from Ref. [39]; Copyright (2023), Springer Nature); (c) Cross-stacked plasmonic nanoparticle assemblies enabling mechanically tunable CD and circular-polarization-selective transmission (Reproduced with permission from Ref. [45]; Copyright (2021), Springer Nature); (d) Stretchable bilayer films for multicolor and white CPL generation (Reproduced with permission from Ref. [70]; Copyright (2025), Wiley); (e) Magnetically assembled twisted structures enabling programmable CPL emission and thermally induced handedness inversion (Reproduced with permission from Ref. [46]; Copyright (2025), Wiley).

this strategy. We recently obtained highly oriented Au nanorod-PVA films by stretching a polymer matrix. When two aligned films were stacked with a controlled twist angle, the system produced ultrabroad CD from 200 nm to 2500 nm, with g_{abs} approaching 1.[35] Duan *et al.* used strained conducting polymer films with in-plane hyperbolic optical anisotropy, in which off-axis stacking produced broadband CD beyond discrete molecular or plasmonic absorption bands.[9] Meng *et al.* integrated the LD and LB functions within a flexible film using plasmonic nanoparticle chains to provide LD and stretched polydimethylsiloxane (PDMS) to provide LB, producing tunable near-infrared (NIR) CD with g_{abs} of 1.71.[71]

Twisted-stacking architectures can also convert linearly polarized or anisotropic emission into CPL. We integrated achiral fluorescent films with twist-stacked plasmonic polymer nanocomposite layers. In this decoupled structure, the fluorescent layer determines the emission wavelength, whereas the plasmonic multilayer controls the polarization state. Mechanical rotation or deformation enabled independent tuning of the CPL wavelength, ellipticity, and handedness, giving g_{lum} up to 0.3 in the visible range (Fig. 4d).[70] Li *et al.* developed photoprogrammable CPL patterns in flexible PDMS films by combining magnetic assembly with *in situ* photopolymerization. The oriented polydiacetylene chains provided linearly polarized emission, and the aligned Ag@Fe_3O_4 nanowires acted as an anisotropic phase-retarding layer. This twisted-stacking heterostructure enabled patterned CPL, while the thermochromic transition of polydiacetylene allowed switching of both the emission wavelength and CPL handedness (Fig. 4e).[46] Similar CPL amplification has been

achieved in PVA/CdSe@CdS nanorod assembly heterostructures, where twisted stacking enhances and dynamically controls emission dissymmetry.[10] Twisted-stacking MOF patterns further extended this design to oriented porous crystalline films, producing tunable CPL with g_{lum} values up to 0.4 and programmable encryption patterns.[47]

Together, twisted-stacking strategies offer a versatile route to strong chiroptical responses by coupling linear anisotropies including LB, LD, and linearly polarized emission. This design enables chiral amplification, broad spectral tunability, and mechanical flexibility even when the building blocks are achiral. Compared to the previous two strategies, twisted stacking particularly benefits from the processability of freestanding anisotropic films, which can be transferred, rotated, restacked, or replaced after fabrication. This post-fabrication reconfigurability makes the interlayer orientation and stacking sequence readily accessible as programming parameters, thereby offering greater structural flexibility. However, the resulting optical performance depends strongly on the stacking accuracy and interface quality. Small angular errors, bubbles, wrinkles or local misalignment can reshape the measured spectra. Moreover, because LB and LD can directly contribute to the apparent CD or CPL signals, the resulting chiroptical signals should be interpreted with caution.

Geometric Microstructuring Strategies

Unlike twisted stacking strategies, which rely on the angular coupling of multiple anisotropic layers, geometric microstructuring strategies can encode chirality directly within a single integrated film architecture. Curvature, buckling, wrinkling, asymmetric deposition, and textured layering can break mirror symmetry and create polarization-selective optical responses from achiral building blocks (Fig. 5a).[11,12,72] Compared with molecular or supramolecular approaches, this strategy offers more direct control over the spatial form of chirality and its mechanical reconfiguration.

In mechanically driven systems, strain release converts planar or linearly assembled structures into three-dimensional twisted morphologies. Hwang *et al.* used the sequential asymmetric and biaxial buckling of PDMS to generate three-dimensional chiral microwrinkles, whose handedness and periodicity could be programmed by the strain direction and release sequence.[11] When plasmonic components are incorporated, these buckled morphologies can give rise to strong chi-

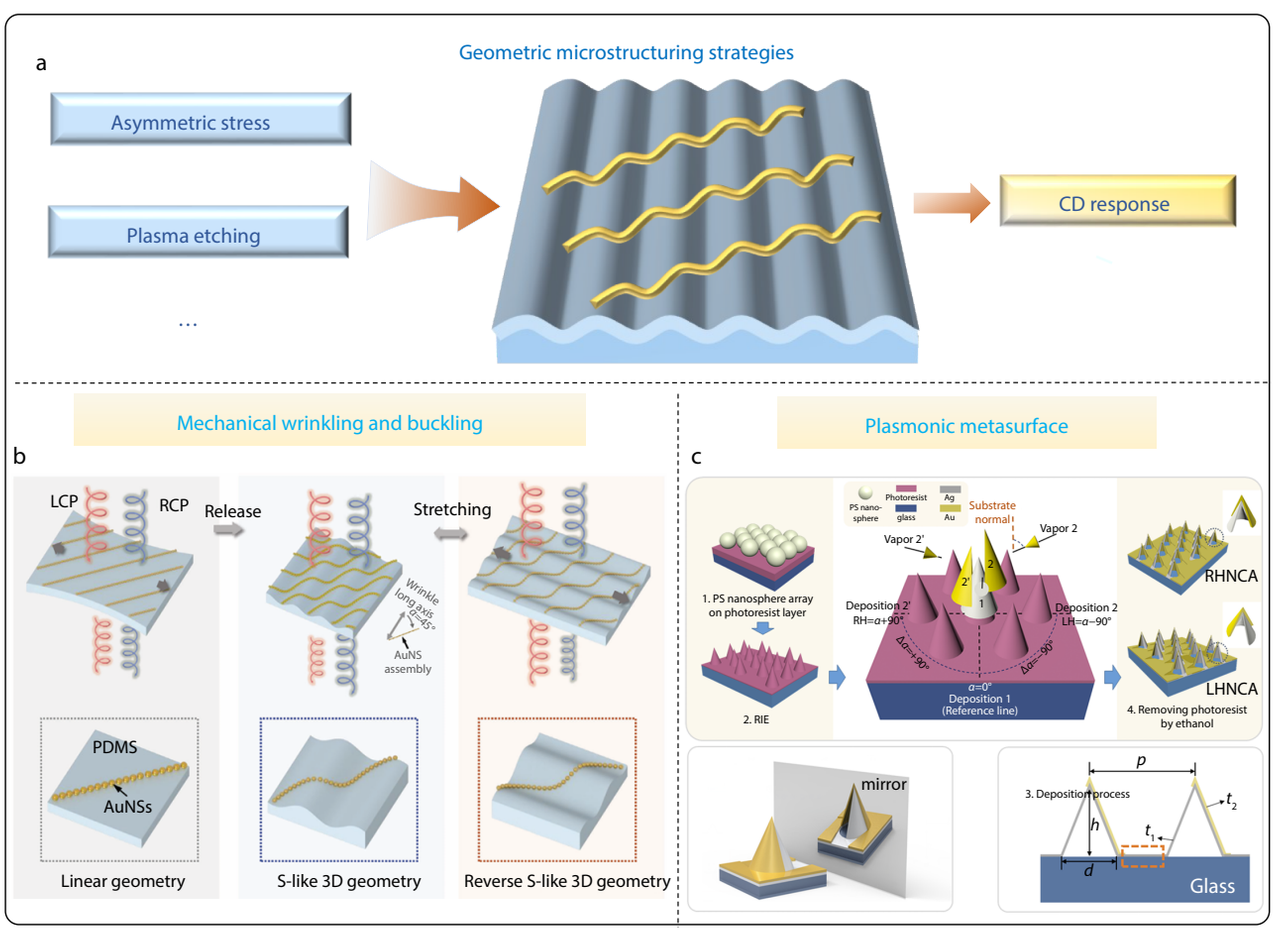


Fig. 5 (a) Schematic illustration of geometric microstructuring, in which mechanical deformation or asymmetric microfabrication generates chiral surface architectures and CD responses; (b) Mechanical buckling transforms linear Au nanosphere chains into switchable S-shaped and reverse-S-shaped chiral architectures (Reproduced with permission from Ref. [12]; Copyright (2025), Wiley); (c) Colloidal lithography and directional metal deposition produce enantiomeric plasmonic nanocone arrays with strong chiroptical responses (Reproduced with permission from Ref. [72]; Copyright (2018), American Chemical Society).

https://doi.org/10.1007/s10118-026-3884-2

roptical signals. He *et al.* assembled gold nanosphere chains on prestretched PDMS; upon strain release, the chains buckled into three-dimensional S-shaped structures and produced tunable CD over the visible-NIR range, with a CD magnitude of 2.6° and g_{abs} up to 0.11 (Fig. 5b).[12] A similar macro-to-nanoscale chirality transfer was demonstrated in reconfigurable nanoparticle-chain nanocomposites, where macroscopic strain gradients produced nonplanar S-like chains and reversible optical rotation.[73] A different route relies on textured layered films rather than on mechanical release. Lu *et al.* fabricated multilayer nanocomposites from achiral 2D nanosheets with complex wrinkled, grooved, or ridged surfaces. These diagonal textures created an angular offset between the LD and LB axes, leading to a strong CD and controllable polarization rotation despite the absence of molecular or nanoscale chirality.[74] Large-area mechanically patterned plasmonic films have further demonstrated that wrinkle-based geometric chirality can be scaled and integrated with polarized emission or information encryption.[75]

Asymmetric deposition and lithographic patterning provide another route for geometrically defined chiral films. Wang *et al.* fabricated centimeter-scale hollow nanocone array films using colloidal lithography followed by oblique Ag/Au deposition. The spatial offset between the two metal shells broke the mirror symmetry and generated asymmetric current oscillations and near-field distributions, giving a pronounced UV-Vis CD response with g_{abs} approaching 10^{-1}. The freestanding films can be transferred onto planar, curved, or flexible substrates, highlighting the integration advantages afforded by detachable chiral metasurfaces (Fig. 5c).[72] Using a related colloidal-lithography strategy, Guan *et al.* simultaneously obtained chiral hollow nanovolcano array films and detachable hollow nanoshells with tunable plasmonic CD.[3] Many chiral metasurfaces have also been reported; however, most of them are surface-bound structures and have not been explicitly demonstrated to be transferable, flexible, or freestanding films. Therefore, these substrate-supported metasurfaces are not discussed in detail herein.[76–78]

Geometric microstructuring strategies provide an integrated route for constructing chiroptical films by encoding the geometric handedness directly into their surface or internal morphologies. The resulting responses could be tuned by varying the strain, curvature, pattern geometry, and deposition direction. Compared with twisted stacking, geometric microstructuring avoids the need for precise interlayer alignment by encoding chirality directly into the film geometry, while placing greater fabrication demands on the precise control of curvature, wrinkle amplitude, pattern geometry, and local structural uniformity. The resulting freestanding structures can be mechanically reconFig.d and conformally integrated with nonplanar surfaces, enabling mechanical adaptability and substrate-independent device integration, which are difficult to achieve with conventional substrate-supported chiroptical films. However, the geometric chirality is highly sensitive to structural defects and processing variations. Achieving large-area uniformity, mechanical stability, and reproducible optical performance remain major challenges. The comparison of the four construction strategies is presented in Table 2.

APPLICATIONS

Once chiroptical responses have been constructed and programmed, FFCFs can function as transferable layers for information encoding, visual conversion, and signal transduction.

Encryption and Anti-counterfeiting

FFCFs are well-suited to encryption and anti-counterfeiting because they can serve as independent, transferable security labels. Their CD or CPL signatures are usually invisible under ordinary observation and require polarization-resolved optical readout, which provides a basis for concealed authentication.[46,59,79] Meanwhile, their flexibility and structural integrity enable cutting, lamination, conformal attachment, and mechanical reconfiguration, thereby introducing additional encoding or decoding keys. This substrate-independent format allows the fabrication and optical characterization of security patterns before integration, thereby decoupling label optimization from the geometry and surface properties of the target object. It also facilitates the modular integration of precharacterized chiroptical layers without modifying the target surface. Based on the optical signal and readout mode, current systems can be broadly grouped into CD-based- and CPL-based strategies.[41,70]

Table 2 Comparative characteristics of the four FFCF construction strategies.

Strategy	Chirality origin	Tuning parameters	Fabrication routes	Key advantages	Main bottlenecks
Multicomponent coupling	Intrinsic chirality of constituent components, transferred or amplified through intercomponent coupling	Composition, temperature, solvent, or mechanical deformation	Solution blending, co-assembly, network formation	Broad chemical/compositional design freedom; modular multifunctionality	Component compatibility and spatial uniformity; migration or phase separation
Helical assembly	Helical order formed through molecular/ nanoscale assembly or chiral polymer conformations	Strain, humidity, solvent, temperature, or light	Self-assembly, liquid-crystal alignment, or helical templating	Chirality amplification; strong stimuli responsiveness	Sensitivity to structural defects, domain alignment, and scattering
Twisted stacking	Macroscopic structural chirality arising from angularly offset anisotropic layers	Twist angle, layer sequence, stacking geometry, or strain	Preparation of anisotropic films followed by controlled angular stacking	High structural programmability; reversible reconfiguration	Precise alignment required; LD/LB artifacts
Geometric microstructuring	Mesoscale geometric chirality encoded in asymmetric surface or internal architectures	Strain, curvature, or deposition direction	Lithography, oblique deposition, wrinkling, or buckling	Integrated chirality encoding; spatial programmability;	Defect sensitivity; limited scalability and reproducibility

https://doi.org/10.1007/s10118-026-3884-2

In CD-based encryption, hidden information is usually encoded as spatial variations in g_{abs}, CD magnitude, or CD sign, while the visible appearance of the film remains nearly unchanged.[29] Lee *et al.* used Au-coated hierarchical chiral plasmonic PDMS films to construct chiral QR code labels, in which opposite-handed patterns yielded distinct spatial g_{abs} maps for polarization-resolved authentication (Fig. 6a).[75] Mechanical modulation can further convert static CD labels into dynamic code. He *et al.* reported flexible chiral plasmonic films based on Au nanosphere assemblies on buckled PDMS substrates, where stretching altered the CD magnitude and handedness, thus enabling switchable information encoding (Fig. 6b).[12] Twist-stacked anisotropic films provide another route for multistate ellipticity encoding. Freestanding and self-healing AgNWs@WPU/TOCNF elastomer films were used to generate twist-angle-dependent ellipticity states, which were used as coding units for matrix encryption (Fig. 6c).[79]

CPL-based strategies extend chiroptical security from absorption-based contrast to multichannel luminescent readouts. In CPL-active films, encoded information can be carried by the emission color, CPL handedness, g_{lum}, afterglow lifetime, or spatial pattern, expanding the readout dimensions beyond absorption dissymmetry.[80,81] Song *et al.* developed chiral superstructure elastomers containing room-temperature phosphorescent polymers, in which reflection color, full-color circularly polarized long-lived phosphorescence, and mechanically tunable g_{lum} jointly enabled dynamic encryption (Fig. 6d).[82] For higher-capacity designs, Feng *et al.* integrated transferable chiroptical layers into a flexible multilayer platform and combined programmable structural coloration with switchable fluorescence and CPL, allowing structural color, fluorescence, and CPL to act as independently address-

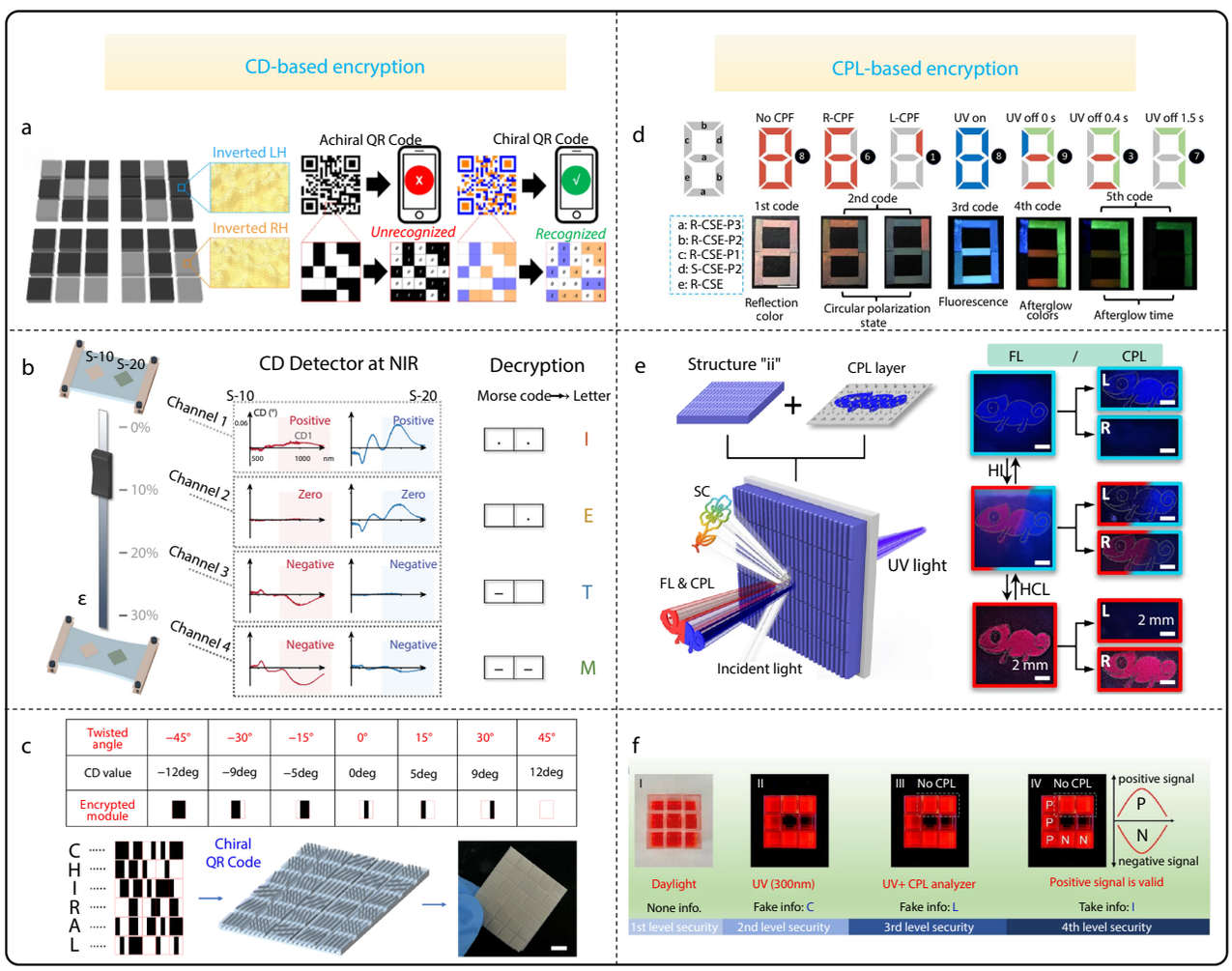


Fig. 6 (a) Chiral QR-code encryption based on large-area plasmonic patterns and spatial gabs mapping (Reproduced with permission from Ref. [75]; Copyright (2023), Springer Nature); (b) Dynamic multichannel encryption in which strain-dependent near-infrared CD states encode Morse-code information (Reproduced with permission from Ref. [12]; Copyright (2025), Wiley); (c) Information encryption and decryption based on the programmable ellipticity of AgNWs@WPU/TOCNF films (Reproduced with permission from Ref. [79]; Copyright (2025), The Royal Society of Chemistry); (d) Multilevel encryption combining reflection color, CPL state, fluorescence, afterglow color, and afterglow lifetime (Reproduced with permission from Ref. [82]; Copyright (2025), Wiley); (e) Multimodal encryption based on structural-color and CPL layers, enabling stimulus-responsive switching and fluorescence and CPL readout (Reproduced with permission from Ref. [41]; Copyright (2025), Springer Nature); (f) Four-level CPL encryption using dye-doped fluorescent films and twisted AuNRs@PVA bilayers (Reproduced with permission from Ref. [70]; Copyright (2025), Wiley).

https://doi.org/10.1007/s10118-026-3884-2

able security channels (Fig. 6e).[41] We further integrated achiral fluorescent layers with twist-stacked plasmonic polymer nanocomposite films to construct freestanding flexible plasmonic multilayer films, enabling independent regulation of the CPL wavelength, handedness, and ellipticity for multilevel matrix encryption (Fig. 6f).[70] In addition to these representative examples, CPL films have also been combined with photochromic switching, long-afterglow readout, mechanical deformation, and humidity-, solvent-, or gas-triggered responses so that identical patterns can display different optical states under different decoding conditions.[37,83–85]

Despite these advances, the broader use of FFCFs in encryption and anti-counterfeiting remains constrained by several practical issues. A central challenge is the balance between concealment and convenient authentication. Highly concealed CD or CPL codes often require polarization-resolved mapping or analysis, and such methods are less suitable for rapid on-site verification. A higher information density also imposes tighter fabrication tolerances because small variations in film thickness, helical pitch, twist angle, interlayer registration, or pixel boundary definition can cause decoding errors. In addition, repeated mechanical operations can introduce reliability problems, including mechanical fatigue, interfacial slippage, photobleaching, humidity sensitivity, and signal drift during repeated deformation or long-term storage. Future developments should therefore prioritize scalable patterning, quantitative quality control, simplified readout, and long-term stability under realistic handling conditions.

Display and Visualization

FFCFs can also function as display layers or polarization-to-image conversion modules. Unlike encryption and anti-counterfeiting, chiroptical signals are mainly used for concealment, display, and visualization, emphasizing the conversion of CPL or polarization-selective responses into observable optical outputs, including color changes, brightness contrast, separated images, and depth perception. The freestanding and mechanically deformable nature of FFCFs permits post-fabrication orientation, stacking, and reshaping, thereby providing additional control over polarization channel separation, image contrast, and spatial optical output without requiring the underlying display substrate to be redesigned. Current studies mainly follow two directions: stereoscopic and depth displays based on left- and right-handed circular polarization channels[42,86] and polarization-to-image visualization that translates invisible chiral optical information into spatially resolved visual patterns.[87]

For stereoscopic and depth displays, FFCFs can separate the left- and right-handed circular polarization channels to deliver different images to the two eyes, thereby generating binocular disparity. Zhan *et al.* demonstrated full-color 3D laser displays using inkjet-printed cholesteric liquid-crystal microlaser arrays in which RGB circularly polarized laser pixels provided polarization-separated image channels for stereoscopic viewing (Fig. 7a).[88] To move this concept to flexible and printable formats, Zhang *et al.* developed CPL-active photonic paints based on chiral liquid-crystal assemblies, which can be printed as full-color pixel arrays on stretchable panels and textiles, forming a flexible chiral photonic device for stereoscopic 3D imaging (Fig. 7b).[43] Guo *et al.* subsequently integrated multilayered circularly polarized electroluminescent microdevices into flexible spatial display panels, enabling the electrically driven control of depth cues and interactive 3D visualization (Fig. 7c).[42] These examples show that circular polarization can serve not only as an optical signal but also as a channel-separation mechanism for flexible depth displays.

For polarization-to-image visualization, FFCFs can convert invisible CPL or polarization contrasts into spatially resolved optical patterns. Yu *et al.* reported mechanically twisted luminescent fibers with full-color and handedness-tunable CPL, which could be embroidered into textiles to display different patterns under unpolarized and circular-polarization-resolved observations.[89] Zhang *et al.* developed freestanding polarized optical mappers based on chiral spin-constrained assemblies embedded in peelable PVA films, enabling background-suppressed pattern recognition and near-field identification through differential LCP/RCP imaging (Fig. 7d).[90] Zhao *et al.* further constructed covalent-bonding chiroptical network films and fibers that maintained CPL contrast under deformation and enabled wearable circular-polarization-differential imaging in complex environments (Fig. 7e).[87] These studies highlight the role of freestanding chiroptical films as visual conversion layers that translate polarization information into readable images.

At the device level, the main bottleneck is the maintenance of the programmed visual state after film processing and integration. For stereoscopic displays, channel fidelity is critical: partial loss of circular polarization, imbalance among color or depth pixels, and imperfect optical alignment can reduce the depth contrast and introduce crosstalk. For polarization-to-image visualization, reliable operation requires stable calibration under non-ideal conditions because deformation, surface roughness, scattering backgrounds, and ambient light may alter the LCP/RCP differential contrast. Therefore, moving these systems toward practical visual modules will require reproducible large-area patterning, optical encapsulation, and integration schemes that preserve the polarization contrast during bending, wearable operation, or electrical driving.

Detection

In detection, FFCFs act as transduction layers that convert the handedness of light into measurable electrical[91] thermal[92] or optical signals.[93] CPL detection mainly involves distinguishing LCP and RCP inputs under controlled optical conditions.[94] Accordingly, FFCF-based CPL detectors should be evaluated using mode-specific metrics, polarization discrimination, response time, and operational stability under mechanical deformation. (R2C4) Their freestanding nature allows the chiroptical layer to be independently characterized, transferred, and integrated with different signal-conversion components, thereby separating the polarization selection from the downstream signal conversion and readout.

For CPL detection, FFCFs convert LCP and RCP inputs into distinguishable photocurrents or other measurable responses, commonly evaluated by the photocurrent dissymmetry factor $g_{ph} = 2\,(I_L - I_R) / (I_L + I_R)$, where I_L and I_R are the photocurrents under LCP and RCP illumination, respectively.[95] Gao *et al.* developed flexible organic phototransistors based on the

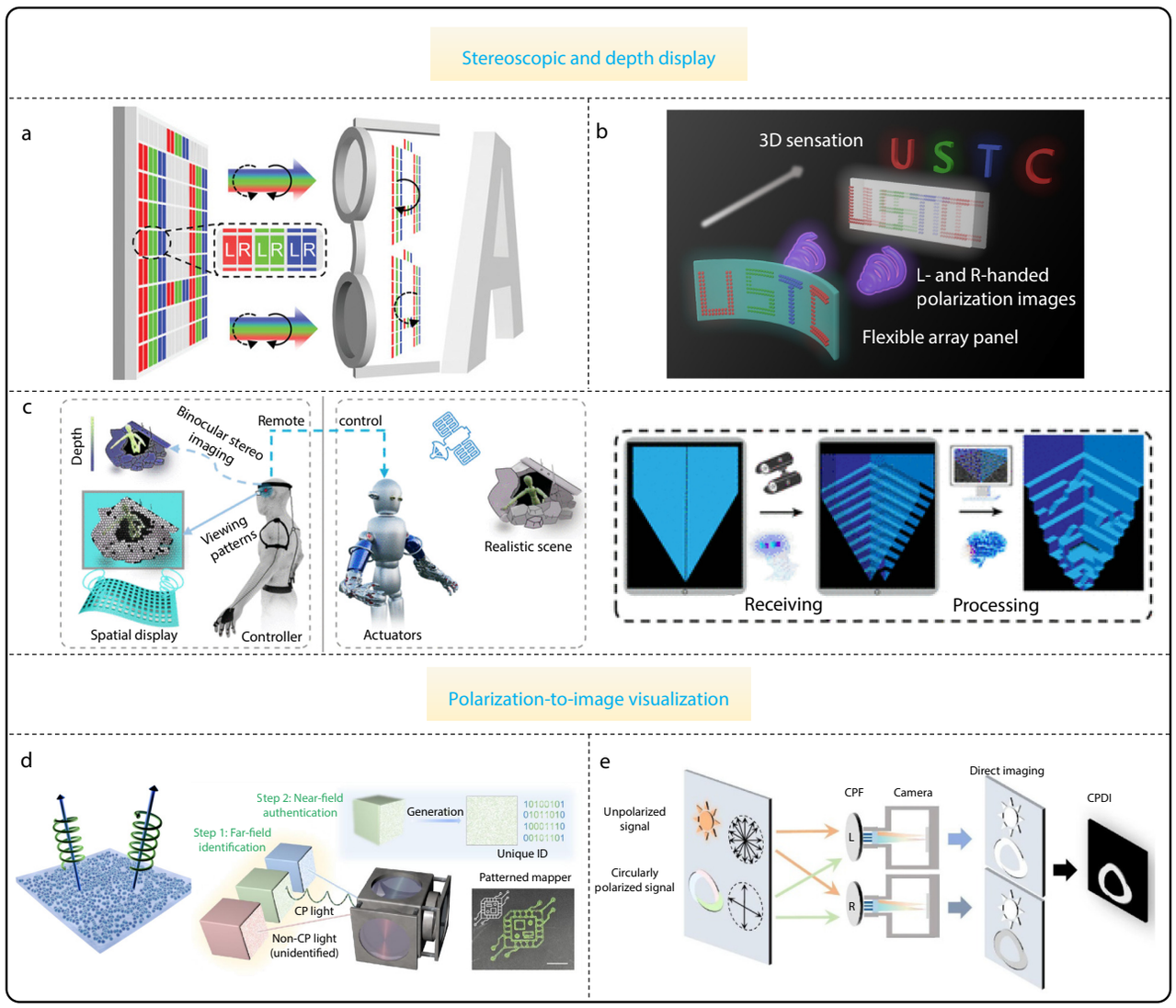


Fig. 7 (a) Schematic of a polarization-multiplexed stereoscopic display that delivers separate left- and right-eye images (Reproduced with permission from Ref. [88]; Copyright (2021), Wiley); (b) Flexible three-dimensional display based on left- and right-handed circularly polarized images (Reproduced with permission from Ref. [43]; Copyright (2023), The American Association for the Advancement of Science); (c) Polarization-assisted depth perception, immersive spatial display, and three-dimensional image acquisition and processing (Reproduced with permission from Ref. [42]; Copyright (2025), The American Association for the Advancement of Science); (d) Chiral photonic platform enabling far-field identification, near-field authentication, and polarization-encoded information extraction (Reproduced with permission from Ref. [90]; Copyright (2025), The American Association for the Advancement of Science); (e) Direct visualization of circularly polarized signals using circular-polarization filters and camera-based polarization-resolved imaging (Reproduced with permission from Ref. [87]; Copyright (2025), Springer Nature).

chiral n-type conjugated polymer P(NDI2MH-T2), achieving reliable CPL discrimination with $|g_{ph}|$ = 0.043 under bending conditions (Fig. 8a).[96] Instead of relying on an intrinsically chiral semiconductor, Feng *et al.* coupled freestanding cholesteric liquid-crystal polymer films with perovskite single-crystal photodetectors, using the film as a CPL-selective optical layer, to obtain a $|g_{ph}|$ of up to 1.95 (Fig. 8b).[97] Lee *et al.* further integrated cholesteric liquid-crystal network films with $MoTe_2/MoS_2$ p-n heterostructures. These films selectively transmitted one circular polarization state, while the 2D heterostructure converted the transmitted light into a photocurrent, giving opposite responses for LCP and RCP and a fast photoresponse of 4 μs.[94] Interlayer-polymerized chiral 2D perovskite single-crystal films provide another route, in which polymerization improves the mechanical and environmental stability while preserving the CPL-selective photoresponse (Fig. 8c).[38] Beyond electronic photodetection, Li *et al.* constructed a freestanding cholesteric liquid crystal–liquid crystal elastomer (CLC-LCE) bilayer for thermal CPL discrimination. The right-handed CLC layer transmitted 89% of the LCP, but only 3% of the RCP at 488 nm, creating a large difference in optical power reaching the photothermal LCE layer. Under LCP illumination, the film temperature increased from 24.5 °C to 71.0 °C as the power density rose from 0 mW·cm^{-2} to 40 mW·cm^{-2}, demonstrating efficient conversion of polarization-dependent transmission into a thermal response. The accompanying deformation served as a secondary macroscopic readout (Fig. 8d).[92] In contrast to the photothermal

route, Anusuyadevi *et al.* developed flexible CNC/glucose chiral photonic films coupled with a birefringent liquid-crystal layer, which translated LCP and RCP illumination into distinct reflection spectra and structural colors, enabling the direct all-optical discrimination of CPL handedness.[98]

Overall, FFCF-based CPL detectors combine polarization selectivity and mechanical adaptability. However, reliable discrimination requires the polarization-dependent output to be separated from the background signals and modality-specific noise. A large output asymmetry alone does not guarantee practical performance if the response is unstable, poorly reproducible, or altered by the film deformation and device integration. Therefore, future studies should prioritize calibrated LCP/RCP measurements, background correction, deformation-independent operation, response stability, and reproducibility under realistic illumination conditions.

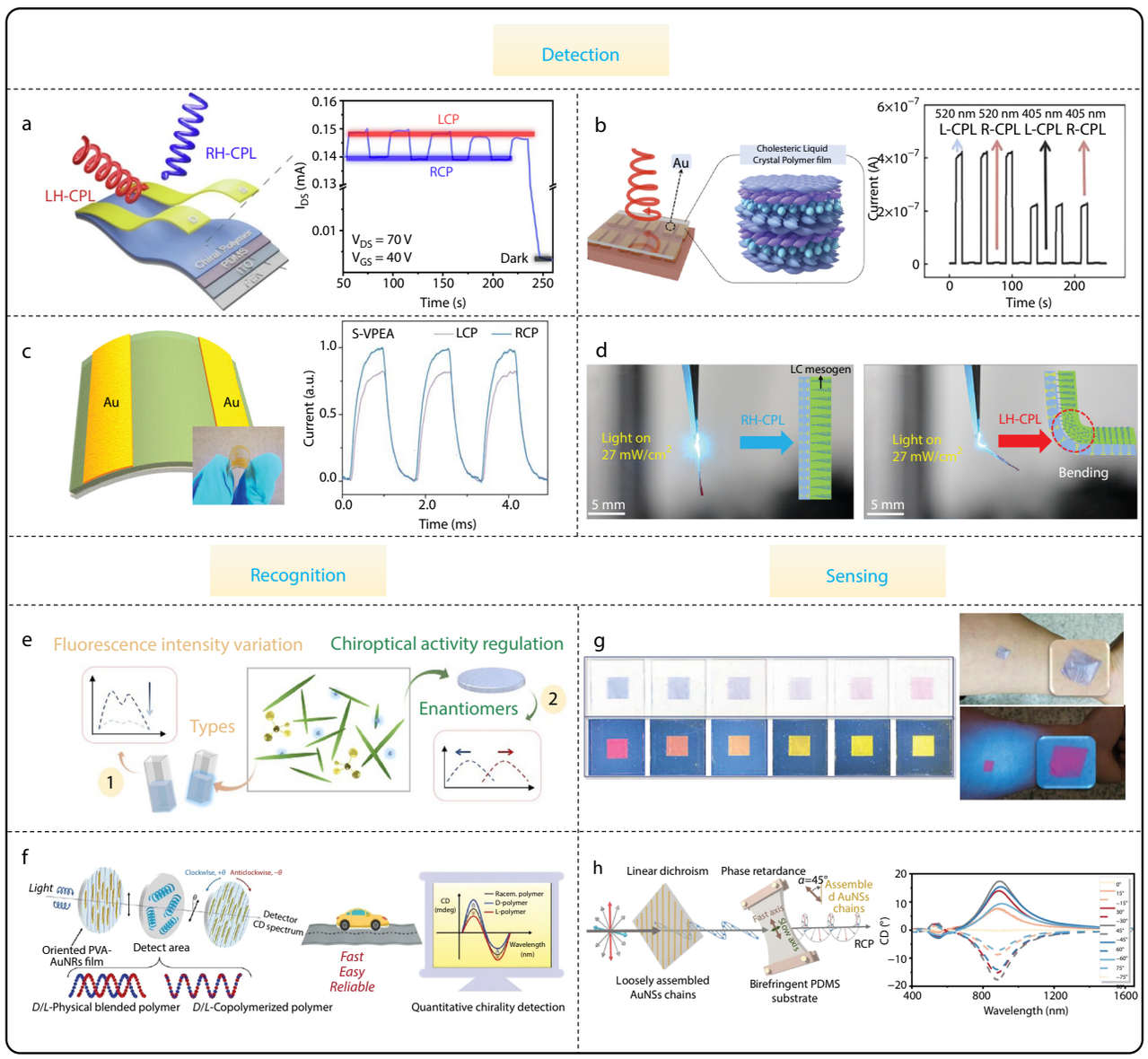


Fig. 8 (a) Flexible CPL photodetector and its distinct photocurrent responses under LCP and RCP illumination (Reproduced with permission from Ref. [96]; Copyright (2025), Springer Nature); (b) Cholesteric liquid-crystal polymer film-integrated photodetector for wavelength- and handedness-dependent CPL detection (Reproduced with permission from Ref. [97]; Copyright (2025), Wiley); (c) Flexible chiral photodetector and its rapid polarization-dependent current responses (Reproduced with permission from Ref. [38]; Copyright (2023), Wiley); (d) Thermal CPL discrimination using a flexible CLC-LCE bilayer, where polarization-selective transmission produces different photothermal outputs and a secondary bending response under LCP illumination (Reproduced with permission from Ref. [92]; Copyright (2023), Wiley); (e) Enantiomer recognition through combined fluorescence-intensity changes and chiroptical responses (Reproduced with permission from Ref. [101]; Copyright (2024), The Royal Society of Chemistry); (f) Quantitative chirality analysis of polymers using twist-stacked PVA-Au nanorod films (Reproduced with permission from Ref. [35]; Copyright (2025), Wiley); (g) Wearable optical sensing of lactate enantiomers using a flexible chiral membrane (Reproduced with permission from Ref. [102]; Copyright (2023), Wiley); (h) Strain-responsive chiroptical sensing based on linearly assembled Au nanoparticle chains on a birefringent polymer film (Reproduced with permission from Ref. [71]; Copyright (2025), Springer Nature).

https://doi.org/10.1007/s10118-026-3884-2

Recognition and Sensing

Molecular and enantiomer recognition using FFCFs focuses on identifying the molecular species or stereochemical configurations through chiroptical changes.[99] By contrast, sensing places greater emphasis on calibrated quantitative readout under more complex conditions, where the target signal may be affected by analyte concentration, environmental variation, mechanical deformation, or optical background.[100] The substrate-independent form of FFCFs leaves both film surfaces accessible to the surrounding medium, facilitating analyte diffusion and interfacial interactions, while minimizing potential interference from a supporting carrier. Additionally, the combination of substrate independence and deformability is particularly advantageous for transferable sensing labels and conformal wearable interfaces.

For molecular and enantiomer recognition, FFCFs translate selective chiral interactions into distinguishable chiroptical or luminescent changes. Wang *et al.* developed CNC/9-aminoacridine co-assembled films that differentiated histidine and tryptophan through photoluminescence variations, and further distinguished their enantiomers through characteristic CD spectral shifts, coupling molecular identification with stereochemical recognition (Fig. 8e).[101] We recently reported twist-stacked PVA-AuNR bilayer films with strong and tunable plasmonic optical activities, where D-, L-, and racemic poly(lactic acid) (PLA) produced distinct CD and g_{abs} responses. The g_{abs} signal varied linearly with the enantiomeric excess, enabling quantitative chirality analysis of the polymer samples (Fig. 8f).[35] Because these systems rely on analyte–film interactions, suppressing nonspecific adsorption and background optical changes is essential for reliable recognition.

For sensing applications, FFCFs are required to provide quantifiable responses to chemical, environmental, or mechanical variables rather than only distinguishing different chiral states. Yang *et al.* developed RT@CDMOF for lactate enantiomer sensing, where fluorescence and reflectance changes enabled dual-channel discrimination and wearable sweat monitoring (Fig. 8g).[102] Mechanical sensing has also been realized in plasmonic chiroptical films, and Meng *et al.* assembled linear Au nanoparticle chains on birefringent polymer films, allowing strain-dependent modulation of CD and polarization rotation with a high g_{abs} of 1.71 in the near-infrared region (Fig. 8h).[71] Structural color shifts provide another common sensing mode for CNC-based chiral photonic films. Dai *et al.* reported CNC-maltodextrin films for detecting water adulteration in ethanol, where water-induced swelling produced rapid reflectance and color changes.[103] Related CNC hydrogels and chiral nematic film systems further convert compression into reversible color and handedness changes for pressure-responsive sensing.[104] These examples show that sensing applications place stronger demands on the calibration stability, reversibility, and interference resistance.

The principal limitation of recognition and sensing lies in distinguishing target-specific responses from nonspecific changes caused by competing species, environmental fluctuations, or mechanical deformation of the film, while maintaining reliable concentration-dependent calibration. Pronounced CD, CPL, fluorescence, and structural color changes do not necessarily indicate reliable sensing without adequate selectivity, quantitative calibration, reversibility, and reproducibility. Therefore, future work should emphasize interference-resistant recognition, concentration-dependent calibration, cycling stability, and batch-to-batch consistency in complex and realistic sample environments.

CONCLUSIONS AND PERSPECTIVES

In summary, this review defines FFCFs as substrate-independent film platforms that combine mechanical deformability with measurable chiroptical activity. Their freestanding nature allows films to be transferred, cut, bent, stretched, folded, or stacked while retaining their optical functions, providing advantages that are difficult to achieve in substrate-bound coatings. Representative systems were organized according to four construction strategies: multicomponent coupling, helical assembly, twisted stacking,

and geometric micro-structuring. These strategies convert molecular chirality, supramolecular organization, optical anisotropy, or geometric asymmetry into CD-, CPL-, and circular-polarization-selective responses. These chiroptical properties can be amplified, tuned, or mechanically reconFig.d by regulating component interactions, helical pitch, interlayer orientation, and surface or internal geometry. These features have enabled applications in information security, display, and visualization, as well as in the detection and analysis of chiral light and matter.

Although considerable progress has been achieved, further development of FFCFs will require addressing several interrelated challenges, including optical characterization, mechanical and structural stability, scalable fabrication, and long-term reliability. On the one hand, the strong linear anisotropy, scattering, surface roughness, and deformation-dependent optical properties of many freestanding films can complicate the assignment of CD and CPL signals. In our recent studies on twist-stacked soft plasmonic films, sample rotation, front-back reversal, and Mueller matrix analysis were combined to distinguish the circular responses from the contributions of linear dichroism and birefringence.[35,70] These approaches improve the reliability of signal assignment; however, standardized characterization protocols are still required across different classes of FFCFs. However, a recurring trade-off can arise between mechanical compliance and structural order: high structural order is generally required for strong and reproducible chiroptical responses, whereas increased mechanical compliance can compromise structural uniformity and chiral ordering, creating a key dilemma for rational FFCFs design. This trade-off becomes particularly important in large-area and scalable fabrication because the helical order, interlayer alignment, multicomponent organization, and geometric microstructures are all sensitive to processing variations and local defects. Addressing these challenges will require scalable fabrication strategies that balance structural order with mechanical compliance. Long-term durability and batch-to-batch reproducibility should be systematically evaluated under repeated deformation and environmental exposure. These efforts are essential for transforming individually optimized demonstrations into reproducible

https://doi.org/10.1007/s10118-026-3884-2

material platforms suitable for practical applications.

BIOGRAPHY

Xi-Chong Ye received his Ph.D. degree in Polymer Chemistry and Physics from Peking University in 2018 under the supervision of Prof. Xinhua Wan. He then conducted postdoctoral research at Peking University from 2019 to 2021. He joined the School of Materials Science and Engineering, Xi'an Jiaotong University, in 2022 and is currently an Associate Professor and Ph.D. supervisor. His research focuses on optically active functional polymers, chiral soft materials, and organic-inorganic hybrid functional materials.

Conflict of Interests

The authors declare no interest conflict.

ACKNOWLEDGMENTS

This work was financially supported by the National Natural Science Foundation of China (No. 52373217) and the Shaanxi Provincial Science and Technology Department (No. 2024GH-ZDXM-15).

REFERENCES

1 Lininger, A.; Palermo, G.; Guglielmelli, A.; Nicoletta, G.; Goel, M.; Hinczewski, M.; Strangi, G. Chirality in light–matter interaction. *Adv. Mater.* **2023**, *35*, 2107325.
2 Fu, W.; Tang, C.; Wang, P. P. Chiral inorganic nanomaterials: exploring new horizons in catalysis through symmetry breaking. *Adv. Mater.* **2026**, *38*, e15236.
3 Guan, Y.; Wang, Z.; Ai, B.; Chen, C.; Zhang, W.; Wang, Y.; Zhang, G. Chiral plasmonic metamaterials with tunable chirality. *ACS Appl. Mater. Interfaces* **2020**, *12*, 50192−50202.
4 Yang, D.; Duan, P.; Zhang, L.; Liu, M. Chirality and energy transfer amplified circularly polarized luminescence in composite nanohelix. *Nat. Commun.* **2017**, *8*, 15727.
5 Cao, M.; Ren, Y.; Wu, Y.; Shen, J.; Li, S.; Yu, Z. Q.; Liu, S.; Li, J.; Rojas, O. J.; Chen, Z. Biobased and biodegradable films exhibiting circularly polarized room temperature phosphorescence. *Nat. Commun.* **2024**, *15*, 2375.
6 Kim, S. U.; Lee, Y. J.; Liu, J.; Kim, D. S.; Wang, H.; Yang, S. Broadband and pixelated camouflage in inflating chiral nematic liquid crystalline elastomers. *Nat. Mater.* **2022**, *21*, 41−46.
7 Kizhakidathazhath, R.; Geng, Y.; Jampani, V. S. R.; Charni, C.; Sharma, A.; Lagerwall, J. P. F. Facile anisotropic deswelling method for realizing large-area cholesteric liquid crystal elastomers with uniform structural color and broad-range mechanochromic response. *Adv. Funct. Mater.* **2020**, *30*, 1909537.
8 Zhou, Y.; Lu, C.; Lu, Z.; Guo, Z.; Ye, C.; Tsukruk, V. V.; Xiong, R. Chiroptical nanocellulose bio-labels for independent multi-channel optical encryption. *Small* **2023**, *19*, 2303064.
9 Duan, Y.; Chen, S.; Jonsson, M. P. Broadband chiroptics with twist-stacked hyperbolic conducting polymer thin films. *Adv. Mater.* **2025**, *37*, e2417024.
10 Wen, L.; Xie, Y.; Yang, P.; Zhang, H.; Li, J.; Feng, Z.; Zou, G. Amplification and dynamic control of circularly polarized luminescence in poly(vinyl alcohol)/CdSe@CdS nanorod assembly twisted-stacking hetero-structures. *Adv. Opt. Mater.* **2024**, *12*, 2301308.
11 Hwang, M.; Kim, C.; Kim, J.; Son, J. G.; Yeom, B. Controlled fabrication of 3D chiral microwrinkles *via* asymmetrical and biaxial bucklings. *Adv. Funct. Mater.* **2019**, *29*, 1808979.
12 He, Y.; Meng, X.; Shen, Z.; Jin, B.; Chen, X.; Ai, B.; Liu, K.; Ye, C. Dynamically tunable chiroptical activities of flexible chiral plasmonic film *via* surface buckling. *Small* **2025**, *21*, 2407635.
13 Fu, R.; Lu, Y.; Cheng, W. Soft plasmonics: design, fabrication, characterization, and applications. *Adv. Opt. Mater.* **2022**, *10*, 2101436.
14 Jia, S.; Tao, T.; Xie, Y.; Yu, L.; Kang, X.; Zhang, Y.; Tang, W.; Gong, J. Chirality supramolecular systems: helical assemblies, structure designs, and functions. *Small* **2024**, *20*, 2307874.
15 Uceda, R. G.; Míguez-Lago, S.; Cruz, C. M.; Morcillo, S. P.; Álvarez de Cienfuegos, L.; Blanco, V.; Campaña, A. G.; Ribagorda, M.; Miguel, D.; Cuerva, J. M. Do's and don'ts when visiting circularly polarized luminescence. *Adv. Opt. Mater.* **2026**, *14*, e03285.
16 Han, Z.; Wang, F.; Sun, J.; Wang, X.; Tang, Z. Recent advances in ultrathin chiral metasurfaces by twisted stacking. *Adv. Mater.* **2023**, *35*, 2206141.
17 Qi, M.; Jing, H.; Duan, P.; Yang, D. Circularly polarized-light-driven chiral optoelectronics: encoding, sensing, and neuromorphic processing from an information-flow perspective. *Mater. Horiz.* **2026**, *13*, 5268−5294.
18 Zhang, M.; Zhuang, T. Processable, high-performance circularly polarized luminescence architectures for information interaction. *Acc. Chem. Res.* **2026**, *59*, 1507−1521.
19 Hu, R.; Lu, X.; Hao, X.; Qin, W. An organic chiroptical detector favoring circularly polarized light detection from near-infrared to ultraviolet and magnetic-field-amplifying dissymmetry in detectivity. *Adv. Mater.* **2023**, *35*, 2211935.
20 Wang, L.; Xue, Y.; Cui, M.; Huang, Y.; Xu, H.; Qin, C.; Yang, J.; Dai, H.; Yuan, M. A chiral reduced-dimension perovskite for an efficient flexible circularly polarized light photodetector. *Angew. Chem. Int. Ed.* **2020**, *59*, 6442−6450.
21 He, S.; Lin, W.; Yu, D.; Shi, J.; Yin, Z.; Sun, C.; Liu, H.; Zhang, C.; Yuan, J.; Bai, S.; Xiao, S.; Long, G.; Yuan, M.; Jiang, Y.; Chen, Y.; Song, Q. Perovskite spin light-emitting diodes with simultaneously high electroluminescence dissymmetry and high external quantum efficiency. *Nat. Commun.* **2025**, *16*, 2201.
22 Li, Z.; Wang, J.; Chi, S.; Lin, K.; Zhang, W.; He, C. Efficient circularly polarized electroluminescence enabled by low-dimensional bichiral perovskite nanocrystals. *ACS Nano* **2024**, *18*, 34962−34970.
23 Zhang, P.; Zhou, G.; de Haan, L. T.; Schenning, A. P. H. J. 4D chiral photonic actuators with switchable hyper-reflectivity. *Adv. Funct. Mater.* **2021**, *31*, 2007887.
24 Ma, J.; Yang, Y.; Valenzuela, C.; Zhang, X.; Wang, L.; Feng, W. Mechanochromic, shape-programmable and self-healable cholesteric liquid crystal elastomers enabled by dynamic covalent boronic ester bonds. *Angew. Chem. Int. Ed.* **2022**, *61*, e202116219.
25 Lv, J.; Gao, X.; Tang, Z. Bioinspired chiral photonic crystals. *Sci. China Mater.* **2025**, *68*, 979−997.
26 Won, Y.; Lee, J.; Lee, Y. H.; Oh, J. H. Chirality transfer and induction across multiscales using chiral plasmonic structures and macroscopic deformation. *Acc. Chem. Res.* **2026**, *59*, 13−26.
27 Grzelak, D.; Tupikowska, M.; Vila-Liarte, D.; Beutel, D.; Bagiński, M.; Parzyszek, S.; Góra, M.; Rockstuhl, C.; Liz-Marzán, L. M.; Lewandowski, W. Liquid crystal templated chiral plasmonic

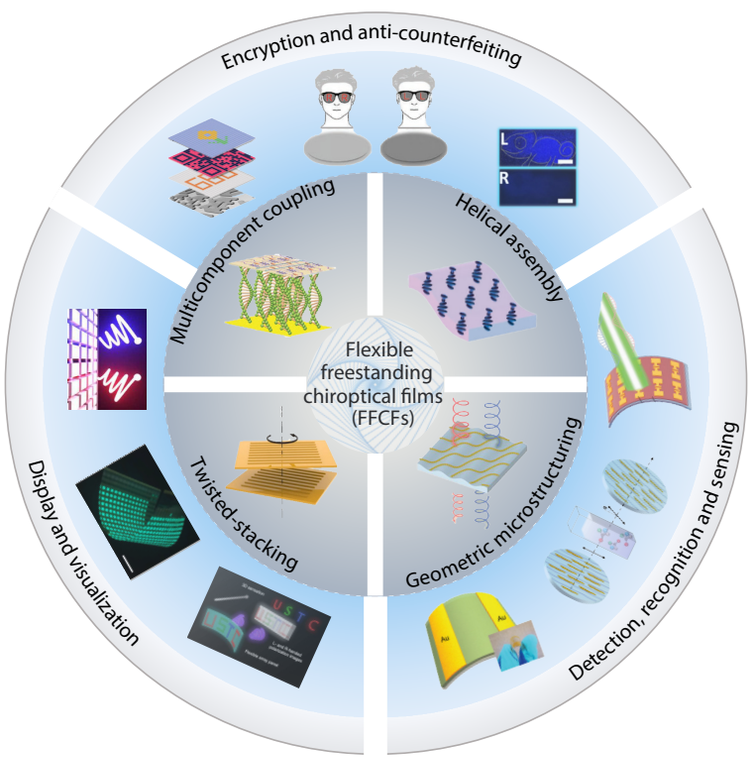
Graphical Abstract

Flexible Freestanding Chiroptical Films: Construction Strategies, Chiroptical Programming, and Applications

Pan-Yi Xi, Sheng-Dan Xie, Yi-Yang Kang, and Xi-Chong Ye

Xi'an Jiaotong University; Shaanxi University of Science and Technology

This review establishes flexible freestanding chiroptical films as distinct material platforms, defining their scope, key metrics, characterization requirements, and four construction strategies. It compares the structural features, tunability, advantages, and limitations of these strategies and summarizes emerging applications in encryption, visualization, detection, recognition, and sensing across diverse material systems.



Chinese J. Polym. Sci. 2026 *https://doi.org/10.1007/s10118-026-3884-2*

films with dynamic tunability and moldability. *Adv. Funct. Mater.* **2022**, *32*, 2111280.

28 Huang, S.; Yu, H.; Li, Q. Supramolecular chirality transfer toward chiral aggregation: asymmetric hierarchical self-assembly. *Adv. Sci.* **2021**, *8*, 2002132.

29 Zhang, X.; Xu, Y.; Valenzuela, C.; Zhang, X.; Wang, L.; Feng, W.; Li, Q. Liquid crystal-templated chiral nanomaterials: from chiral plasmonics to circularly polarized luminescence. *Light Sci. Appl.* **2022**, *11*, 223.

30 Li, Z.-Q.; Zhang, D.-C.; Wang, H.-X.; Li, M.; Jiang, W.; Zhang, Y.; Huang, Z.; Zhong, H.; Wei, N.-X.; Dong, X.; Zhao, W.; Ji, H.; Yuan, L.; Zhou, Z.; Zhang, J.; Zhang, M.; Li, S.; Li, L.; Gu, Z.-G.; Qiu, Z.; Zhao, B.; Wang, Z.; Ma, X.; Cheng, Y.; Deng, J.; Zhang, J.; Zang, S.-Q.; Long, G.; Duan, P.; Chen, C.-F.; Zheng, Y.-X.; Zhao, Y.-S.; Luo, J.; Chen, R.; Zhuang, T.; Zhong, Y.-W.; Tang, B.-Z.; Liu, M. Circularly polarized luminescence: materials, photophysics, devices, and applications. *Sci. China Chem.* **2026**, *69*, 2127–2192.

31 Zhang, R.; Zhong, H.; Yang, K.; Pan, K.; Zhao, B.; Deng, J. Energy transfer for constructing circularly polarized luminescence materials: recent progress and future prospects. *Adv. Funct. Mater.* **2025**, *35*, 2417308.

32 Zhong, H.; Gao, X.; Zhao, B.; Deng, J. "Matching rule" for generation, modulation and amplification of circularly polarized luminescence. *Acc. Chem. Res.* **2024**, *57*, 1188–1201.

33 Wang, Y.; Wu, Z.; Yu, W.; Liu, Z. Recent progresses and applications on chiroptical metamaterials: a review. *J. Phys. D Appl. Phys.* **2024**, *57*, 493004.

34 Chen, R.; Jiang, S.; Zhang, X.; Yang, W.; Xie, Z.; Lin, Y.; Zhu, Y.; Liu, J.; Zhu, W.; Jiang, W.; Liu, S.; Xiong, B.; Yan, Y.; Cai, B.; Gu, Z.; Yang, S.; Zhang, N.; Liang, C. Multidimensional symmetry engineering of metasurfaces for circular dichroism and advanced photonics. *Adv. Mater.* **2026**, *38*, e74368.

35 Xi, P.; Zhao, W.; Cao, Y.; Xie, S.; Wang, P.; Ungar, G.; Ye, X.; Liu, F. Facile construction of soft plasmonic sensors with exceptional optical activity for quantitative chiral detection. *Small* **2025**, *21*, 2408176.

36 Duan, H.; Zhao, J.; Li, S.; Qi, D.; Li, J. Flexible anti-counterfeiting circularly polarized luminescent elastomer from supramolecular polyurethanes. *Adv. Opt. Mater.* **2024**, *12*, 2400379.

37 Zhao, S.; Li, G.; Guo, Q.; Wang, Y.; Zhang, M.; Zhou, Y.; Jin, S.; Zhu, M.; Zhuang, T. Visualizing circularly polarized long afterglow for information security. *Adv. Opt. Mater.* **2023**, *11*, 2202933.

38 Zhao, Y.; Yin, X.; Gu, Z.; Yuan, M.; Ma, J.; Li, T.; Jiang, L.; Wu, Y.; Song, Y. Interlayer polymerization of 2D chiral perovskite single-crystal films toward high-performance flexible circularly polarized light detection. *Adv. Funct. Mater.* **2023**, *33*, 2306199.

39 Xie, Y.; Feng, S.; Deng, L.; Cai, A.; Gan, L.; Jiang, Z.; Yang, P.; Ye, G.; Liu, Z.; Wen, L.; Zhu, Q.; Zhang, W.; Zhang, Z.; Li, J.; Feng, Z.; Zhang, C.; Du, W.; Xu, L.; Jiang, J.; Chen, X.; Zou, G. Inverse design of chiral functional films by a robotic AI-guided system. *Nat. Commun.* **2023**, *14*, 6177.

40 Shi, Y.; Han, J.; Li, C.; Zhao, T.; Jin, X.; Duan, P. Recyclable soft photonic crystal film with overall improved circularly polarized luminescence. *Nat. Commun.* **2023**, *14*, 6123.

41 Feng, Z.; Li, J.; Yang, P.; Xu, X.; Wang, D.; Li, J.; Zhang, C.; Li, J.; Zhang, H.; Zou, G.; Chen, X. Dynamic multimodal information encryption combining programmable structural coloration and switchable circularly polarized luminescence. *Nat. Commun.* **2025**, *16*, 2264.

42 Guo, Q.; Li, Z.; Zhou, Y.; Zhao, S.; Wang, Y.; Zhang, M.; Li, G.; Tong, Z.; Zhuang, T.; Yu, S.-H. Self-positioning microdevices enable adaptable spatial displaying. *Sci. Adv.* **2025**, *11*, eadv2721.

43 Zhang, M.; Guo, Q.; Li, Z.; Zhou, Y.; Zhao, S.; Tong, Z.; Wang, Y.; Li, G.; Jin, S.; Zhu, M.; Zhuang, T.; Yu, S.-H. Processable circularly polarized luminescence material enables flexible stereoscopic 3D imaging. *Sci. Adv.* **2023**, *9*, eadi9944.

44 Pan, Y.; Wang, T.; Wang, R.; Wang, H.-X.; Liu, M. Cascading chirality from molecule to twisted microstructures with amplified circularly polarized luminescence. *Nat. Commun.* **2026**, *17*, 1786.

45 Probst, P. T.; Mayer, M.; Gupta, V.; Steiner, A. M.; Zhou, Z.; Auernhammer, G. K.; König, T. A. F.; Fery, A. Mechano-tunable chiral metasurfaces *via* colloidal assembly. *Nat. Mater.* **2021**, *20*, 1024–1028.

46 Li, J.; Feng, Z.; Zhang, C.; Hu, J.; Wang, D.; Xie, Y.; Li, J.; Li, J.; Zhang, H.; Zou, G. Magnetic assembly-assisted photoprogrammable circularly polarized luminescence patterns in flexible PDMS films. *Adv. Funct. Mater.* **2025**, *35*, 2501168.

47 Chu, X.; Li, J.; Wang, D.; Gan, L.; Liu, X.; Feng, Z.; Yang, P.; Zhang, H.; Xie, Y.; Wang, F.; Zou, G. Twisted-stacking MOF patterns with tailorable circularly polarized luminescence properties and encryption applications. *Nat. Commun.* **2025**, *16*, 10347.

48 Tan, L.; Fu, W.; Gao, Q.; Wang, P.-P. Chiral plasmonic hybrid nanostructures: a gateway to advanced chiroptical materials. *Adv. Mater.* **2024**, *36*, 2309033.

49 Lv, J.; Yang, X.; Tang, Z. Rational design of all-inorganic assemblies with bright circularly polarized luminescence. *Adv. Mater.* **2023**, *35*, 2209539.

50 Mitov, M. Cholesteric liquid crystals with a broad light reflection band. *Adv. Mater.* **2012**, *24*, 6260–6276.

51 Kitzmann, W. R.; Freudenthal, J.; Reponen, A. M.; VanOrman, Z. A.; Feldmann, S. Fundamentals, advances, and artifacts in circularly polarized luminescence (CPL) spectroscopy. *Adv. Mater.* **2023**, *35*, 2302279.

52 Lu, H.; Di Bari, L.; Favereau, L. Standardizing the characterization of circularly polarized luminescence of chiral materials. *Nat. Photon.* **2025**, *19*, 1041–1047.

53 Baguenard, B.; Bensalah-Ledoux, A.; Guy, L.; Riobé, F.; Maury, O.; Guy, S. Theoretical and experimental analysis of circularly polarized luminescence spectrophotometers for artifact-free measurements using a single CCD camera. *Nat. Commun.* **2023**, *14*, 1065.

54 Tang, X.; Zhang, K.; Xue, R.; Zheng, Y.; Chen, S.; Zheng, S.; Fan, J.; Zhang, Y.; Ye, W.; Zhang, W.; Cai, S.; Liu, Y. Frontispiece: self-standing chiral covalent organic framework thin films with full-color tunable guest-induced circularly polarized luminescence. *Angew. Chem. Int. Ed.* **2024**, *63*, e202485061.

55 Guo, G.; Li, H.; Yan, Y.; Zhao, W.; Gao, Z.; Cao, H.; Yan, X.; Li, H.; Xie, G.; Chen, R.; Tao, Y.; Huang, W. A dynamic H-bonding network enables stimuli-responsive color-tunable chiral afterglow polymer for 4D encryption. *Adv. Mater.* **2024**, *36*, 2412100.

56 Duan, H.; Li, S.; Wu, X.; Deng, J.; Li, J.; Qi, D.; Zhao, B. Solvent-free supramolecular polymerization for feather-like nanostructured chiral fluorescent polyurethanes with multimodal chiroptical stimuli responsiveness. *Adv. Sci.* **2025**, *12*, 2417572.

57 Chen, R.; Feng, R.; Huang, Z.; Feng, D.; Long, Y.; Zhang, J.; Yang, Y.; Ma, Z.; Yuan, Z.; Lu, S.; Zhao, Z.; Chen, X. Chiral polymer-organic molecule composite with circularly polarized thermally activated delayed fluorescence and room-temperature phosphorescence by bridging effect of hydrogen bond. *Adv. Funct. Mater.* **2024**, *34*, 2404602.

58 Nie, F.; Yan, D. Bio-sourced flexible supramolecular glasses for dynamic and full-color phosphorescence. *Nat. Commun.* **2024**, *15*, 9491.

59 Li, N.; Chang, L.-M.; Gu, Z.-G.; Zhang, J. Chiral noncovalent peptide glasses for highly circularly polarized luminescence. *Adv. Mater.* **2026**, *38*, e12857.

60 Fu, K.; Zhao, Y.; Liu, G. Pathway-directed recyclable chirality inversion of coordinated supramolecular polymers. *Nat. Commun.* **2024**, *15*, 9571.

61 Qi, W.; Ma, C.; Liao, P.; Li, H.; Gu, T.; Wu, T.; Huang, J.; Yan, Y. Unprecedented thermo-enhanced retainable circularly polarized luminescence. *Adv. Opt. Mater.* **2023**, *11*, 2201229.

62 Xiao, Y. H.; Weidler, P.; Lin, S.-S.; Wöll, C.; Gu, Z. G.; Zhang, J. Chiral metal-organic cluster induced high circularly polarized luminescence of metal-organic framework thin film. *Adv. Funct. Mater.* **2022**, *32*, 2204289.

63 Xiao, Y. H.; Ma, Z. Z.; Yang, X. X.; Li, D. S.; Gu, Z. G.; Zhang, J. Inducing circularly polarized luminescence by confined synthesis of ultrasmall chiral carbon nanodot arrays in pyrene-based MOF thin film. *ACS Nano* **2023**, *17*, 19136–19143.

64 Wang, N.; Hong, R.; Zhang, G.; Pan, M.; Bao, Y.; Zhang, W. Molecular imprinting strategy enables circularly polarized luminescence enhancement of recyclable chiral polymer films. *Small* **2025**, *21*, 2409078.

65 Qin, W.; Li, J.; Li, C.; Zeng, Q.; Teng, Q.; Yang, Y.; Li, J.; Liao, K.; Hou, M.; Tan, Q.; Xu, X.; Chen, Y.; Hu, Y.; Zeng, Z.; Zhang, X.; Yuan, F. Helical nanoconfinement in recyclable chiral soft photonic crystals enables strong and efficient full-color circularly polarized luminescence from carbon quantum dots.

Angew. Chem. Int. Ed. **2026**, *65*, e4885590.
66 Liu, J.; Zhang, S.; Wang, Z.; Xia, X.; Zhang, J.; Yu, Y.; Xiao, Y.; Ren, Y.; Chen, J.; Yang, B.; Xie, W.; Hu, W.; Yang, H. Visible-light-programmed patterning in dynamically bonded cholesteric liquid crystal elastomer. *Nat. Commun.* **2024**, *15*, 10367.
67 Hussain, S.; Park, S. Y. Photonic cholesteric liquid-crystal elastomers with reprogrammable helical pitch and handedness. *ACS Appl. Mater. Interfaces* **2021**, *13*, 59275−59287.
68 Nam, S.; Jung, W.; Shin, J. H.; Choi, S. S. Omnidirectional color wavelength tuning of stretchable chiral liquid crystal elastomers. *Light Sci. Appl.* **2024**, *13*, 114.
69 Choi, Y. J.; Lee, J. J.; Park, J. S.; Kang, H.; Kim, M.; Kim, J.; Okada, D.; Kim, D. H.; Araoka, F.; Choi, S.-W. Circularly polarized light emission from nonchiral perovskites incorporated into nanoporous cholesteric polymer templates. *ACS Nano* **2024**, *18*, 909−918.
70 Xi, P.; Wang, F.; Xie, S.; Wang, P.; Zhang, S.; Ye, X.; Ungar, G.; Liu, F. Fully tunable circularly polarized light from achiral soft plasmonic multilayers. *Laser Photonics Rev.* **2025**, *19*, e01294.
71 Meng, X.; He, Y.; Dimitrov, B.; Jin, B.; Zhu, Z.; Yuan, L.; Tsukruk, V. V.; Ye, C. Dynamic mechanical modulation of chiroptical structures *via* linearly assembled plasmonic nanoparticles on birefringent polymer films. *Nat. Commun.* **2025**, *16*, 5156.
72 Wang, Z.; Ai, B.; Zhou, Z.; Guan, Y.; Möhwald, H.; Zhang, G. Free-standing plasmonic chiral metamaterials with 3D resonance cavities. *ACS Nano* **2018**, *12*, 10914−10923.
73 Kim, Y.; Yeom, B.; Arteaga, O.; Yoo, S. J.; Lee, S. G.; Kim, J. G.; Kotov, N. A. Reconfigurable chiroptical nanocomposites with chirality transfer from the macro- to the nanoscale. *Nat. Mater.* **2016**, *15*, 461−468.
74 Lu, J.; Wu, W.; Colombari, F. M.; Jawaid, A.; Seymour, B.; Whisnant, K.; Zhong, X.; Choi, W.; Chalmpes, N.; Lahann, J.; Vaia, R. A.; de Moura, A. F.; Nepal, D.; Kotov, N. A. Nano-achiral complex composites for extreme polarization optics. *Nature* **2024**, *630*, 860−865.
75 Lee, Y. H.; Won, Y.; Mun, J.; Lee, S.; Kim, Y.; Yeom, B.; Dou, L.; Rho, J.; Oh, J. H. Hierarchically manufactured chiral plasmonic nanostructures with gigantic chirality for polarized emission and information encryption. *Nat. Commun.* **2023**, *14*, 7298.
76 Shi, T.; Deng, Z. L.; Geng, G.; Zeng, X.; Zeng, Y.; Hu, G.; Overvig, A.; Li, J.; Qiu, C. W.; Alù, A.; Kivshar, Y. S.; Li, X. Planar chiral metasurfaces with maximal and tunable chiroptical response driven by bound states in the continuum. *Nat. Commun.* **2022**, *13*, 4111.
77 Esposito, M.; Manoccio, M.; Leo, A.; Cuscunà, M.; Sun, Y.; Ageev, E.; Zuev, D.; Benedetti, A.; Tarantini, I.; Passaseo, A.; Tasco, V. 3D chiral MetaCrystals. *Adv. Funct. Mater.* **2022**, *32*, 2109258.
78 Khaliq, H. S.; Nauman, A.; Lee, J. W.; Kim, H. R. Recent progress on plasmonic and dielectric chiral metasurfaces: fundamentals, design strategies, and implementation. *Adv. Opt. Mater.* **2023**, *11*, 2300644.
79 Xi, P.; Cao, Y.; Tan, T.; Ye, X.; Liu, F. Programmable chiroptical multilayer films assembled from self-healing stretchable elastomers for information encryption. *J. Mater. Chem. C* **2025**, *13*, 15398−15406.
80 Liu, J.; Zhou, X. Y.; Wei, J.; Wu, J. J.; Hu, J. X.; Fang, X. Y.; Lan, R. C.; Tao, Y.; Ma, Y.; Li, B. X.; Yang, H.; Lu, Y. Q.; Zhao, Q. Multi-color circularly polarized room-temperature phosphorescence from processable chiral photonic films. *Adv. Funct. Mater.* **2025**, *35*, 2506911.
81 Lin, S.; Tang, Y.; Kang, W.; Bisoyi, H. K.; Guo, J.; Li, Q. Photo-triggered full-color circularly polarized luminescence based on photonic capsules for multilevel information encryption. *Nat. Commun.* **2023**, *14*, 3005.
82 Song, Z. P.; Wei, J.; Liu, J.; Chu, Z. F.; Hu, J. X.; Chakraborty, S.; Ma, Y.; Li, B. X.; Lu, Y. Q.; Zhao, Q. Mechanically-tunable and full-color circularly polarized long-lived phosphorescence in chiral superstructure elastomers. *Adv. Mater.* **2025**, *37*, 2419640.
83 Song, L.; Dong, Y.; Zhao, B.; Wu, Y.; Deng, J. Reversible photochromism for dynamically tuning full-color circularly polarized luminescence toward multi-level anti-counterfeiting application. *Adv. Opt. Mater.* **2024**, *12*, 2400215.
84 Luo, Z. W.; Ji, H.; Jin, X.; Song, J.; Yu, Z.-Q.; Duan, P.; Zhao, T. Mechanically steered photon upconversion and circularly polarized luminescence in stretchable photonic crystal films. *Nat. Commun.* **2025**, *16*, 9960.
85 Jiang, K. J.; Wang, D. M.; Dong, S. S.; Xu, H.; Ding, G. Q.; Yan, Z. H.; Zhang, S.; Huang, C.; Zhao, H. Interfacial modulation of Cu(I) cluster-CNC photonic films for efficient circularly polarized luminescence and multilevel anticounterfeiting. *Adv. Funct. Mater.* **2026**, *36*, e75613.
86 Huang, L.; Chen, X.; Mühlenbernd, H.; Zhang, H.; Chen, S.; Bai, B.; Tan, Q.; Jin, G.; Cheah, K. W.; Qiu, C. W.; Li, J.; Zentgraf, T.; Zhang, S. Three-dimensional optical holography using a plasmonic metasurface. *Nat. Commun.* **2013**, *4*, 2808.
87 Zhao, S.; Zhang, M.; Li, A.; Tong, Z.; Li, G.; Guo, Q.; Zhou, Y.; Wang, Y.; Cai, J.; Zhuang, T. Covalent-bonding chiroptical network structures for circular polarization differential imaging. *Nat. Commun.* **2025**, *16*, 10644.
88 Zhan, X.; Xu, F. F.; Zhou, Z.; Yan, Y.; Yao, J.; Zhao, Y. S. 3D laser displays based on circularly polarized lasing from cholesteric liquid crystal arrays. *Adv. Mater.* **2021**, *33*, 2104418.
89 Yu, X.; Chen, L.; Liu, Q.; Liu, X.; Qiu, Z.; Zhang, X.; Zhu, M.; Cheng, Y. Mechanically twisting-induced top-down chirality transfer for tunable full-color circularly polarized luminescent fibers. *Adv. Sci.* **2025**, *12*, e2412778.
90 Zhang, M.; Zhao, S.; Li, J.; Li, Z.; Cai, J.; Zhou, Y.; Guo, Q.; Gao, W.; Tong, Z.; Wang, Y.; Li, G.; Guo, X.; Li, A.; Lin, J.; Zhuang, T. Chiral spin constrained assemblies for polarized optical mapping. *Sci. Adv.* **2025**, *11*, eady1001.
91 Han, H.; Lee, Y. J.; Kyhm, J.; Jeong, J. S.; Han, J. H.; Yang, M. K.; Lee, K. M.; Choi, Y.; Yoon, T. H.; Ju, H.; Ahn, S. K.; Lim, J. A. High-performance circularly polarized light-sensing near-infrared organic phototransistors for optoelectronic cryptographic primitives. *Adv. Funct. Mater.* **2020**, *30*, 2006236.
92 Li, Y.; Liu, Y.; Luo, D. Circularly polarized light-driven liquid crystal elastomer actuators. *Adv. Opt. Mater.* **2023**, *11*, 2202695.
93 Zheng, H.; Ju, B.; Wang, X.; Wang, W.; Li, M.; Tang, Z.; Zhang, S. X.; Xu, Y. Circularly polarized luminescent carbon dot nanomaterials of helical superstructures for circularly polarized light detection. *Adv. Opt. Mater.* **2018**, *6*, 1801246.
94 Lee, J. J.; Han, S. J.; Choi, C.; Seo, C.; Hwang, S.; Kim, J.; Hong, J. P.; Jang, J.; Kyhm, J.; Kim, J. W.; Yu, B. S.; Lim, J. A.; Wang, G.; Kang, J.; Kim, Y.; Ahn, S. K.; Ahn, J.; Hwang, D. K. Polarization-sensitive in-sensor computing in chiral organic integrated 2D p-n heterostructures for mixed-multimodal image processing. *Nat. Commun.* **2025**, *16*, 4624.
95 Wan, L.; Zhang, R.; Cho, E.; Li, H.; Coropceanu, V.; Brédas, J.-L.; Gao, F. Sensitive near-infrared circularly polarized light detection *via* non-fullerene acceptor blends. *Nat. Photonics* **2023**, *17*, 649−655.
96 Gao, K.; Kim, S.; Zhao, W.; Ye, X.; Wang, P. P.; Liu, L.; Ahn, J.; Zhuo, H.; Li, Z.; Wang, Z.; Chang, G.; Ma, W.; Zhang, M.; Long, G.; Shang, X.; Oh, J. H. High-performance flexible circularly polarized light photodetectors based on chiral n-type naphthalenediimide-bithiophene polymers. *npj Flex. Electron.* **2025**, *9*, 83.

97 Feng, Y.; Gao, G.; Wen, X.; Chen, Z.; Huang, J.; Yang, C.; Jiang, X. F.; Polavarapu, L.; Zhou, G.; Hu, X. Circularly polarized perovskite photodetector with photocurrent dissymmetry factors of up to 1.95 enabled by liquid crystal. *Adv. Funct. Mater.* **2025**, *35*, 2421338.
98 Anusuyadevi, P. R.; Shanker, R.; Cui, Y.; Riazanova, A. V.; Järn, M.; Jonsson, M. P.; Svagan, A. J. Photoresponsive and polarization-sensitive structural colors from cellulose/liquid crystal nanophotonic structures. *Adv. Mater.* **2021**, *33*, 2101519.
99 Wu, X.; Liu, J.; Ni, F.; Jiang, L.; Wei, S.; Wang, X.; Qiu, L. High-performance gas-phase chiral enantiomer detectors based on chiral-induced spin selectivity effect. *Nat. Commun.* **2025**, *16*, 8474.
100 Montes-García, V.; Samorì, P. Humidity sensing with supramolecular nanostructures. *Adv. Mater.* **2024**, *36*, 2208766.
101 Wang, Y.; Zhou, Y.; Zhao, S.; Zhang, M.; Li, A.; Li, G.; Guo, Q.; Guo, X.; Tong, Z.; Li, Z.; Lin, J.; Zhuang, T. Recognizing chiral amino acids with a dual-optical-response system. *J. Mater. Chem. A* **2024**, *12*, 9421−9426.
102 Yang, X. L.; Yang, Z. Y.; Shao, R.; Guan, R. F.; Dong, S. L.; Xie, M. H. Chiral MOF derived wearable logic sensor for intuitive discrimination of physiologically active enantiomer. *Adv. Mater.* **2023**, *35*, 2304046.
103 Dai, M.; Chen, Q.; Zhou, R.; Simal-Gandara, J.; Teng, H.; Chen, L. Bioinspired chiral cellulose nanocrystal photonic films for rapid visual ethanol adulteration detection. *Chem. Eng. J.* **2026**, *529*, 173255.
104 Xu, Y. T.; Li, Z.; Ortiz Medrano, M. A.; MacLachlan, M. J. Unidirectional cellulose nanocrystal hydrogel for bio-based invertible chiral optics and sensors. *Nat. Commun.* **2026**, *17*, 7141.

https://doi.org/10.1007/s10118-026-3884-2